 doi:10.20944/preprints202010.0208.v2

Article

Anthropogenic factors affecting the vegetation dynamics in the arid Middle East

Iman Rousta [1,2], Haraldur Olafsson [3], Hao Zhang [4], Md Moniruzzaman [5], Jaromir Krzyszczak [6,*] and Piotr Baranowski [6]

[1] Department of Geography, Yazd University, Yazd 8915818411, Iran; irousta@yazd.ac.ir
[2] Institute for Atmospheric Sciences-Weather and Climate, University of Iceland and Icelandic Meteorological Office (IMO), Bustadavegur 7, IS-108 Reykjavik, Iceland
[3] Institute for Atmospheric Sciences-Weather and Climate and Department of Physics, University of Iceland and Icelandic Meteorological Office (IMO), Bustadavegur 7, IS-108 Reykjavik, Iceland, Email: haraldur@vedur.is
[4] Department of Environmental Science and Engineering Jiangwan Campus, Fudan University, 2005 Songhu Road,Yangpu District Shanghai 200438, China; zhokzhok@163.com
[5] ASICT Division, Bangladesh Agricultural Research Institute, Gazipur-1701, Bangladesh; moniruzzaman1313ku@gmail.com
[6] Institute of Agrophysics, Polish Academy of Sciences, Doświadczalna 4, 20-290 Lublin, Poland; j.krzyszczak@ipan.lublin.pl, p.baranowski@ipan.lublin.pl
* Corresponding author: Jaromir Krzyszczak, e-mail: j.krzyszczak@ipan.lublin.pl; ORCID ID: 0000-0002-9235-8119, phone: (+48) 817445061, fax: (+48) 81744506

Abstract: The spatiotemporal variability of vegetation in the Middle East was investigated for the period 2001–2019 using the Moderate Resolution Imaging Spectroradiometer (MODIS) 16-day/500 m composites of the Normalized Difference Vegetation Index (NDVI; MOD13A1). The results reveal a strong increase in the NDVI coverage in the Middle East during the study period (R = 0.75, p-value = 0.05). In Egypt, the annual coverage exhibits the strongest positive trend (R = 0.99, p-value = 0.05). In Turkey, both the vegetation coverage and density increased from 2001 to 2019, which can be attributed to the construction of some of the biggest dams in the Middle East, such as the Atatürk and Ilisu dams. Significant increases in the annual coverage and maximum and average NDVI in Saudi Arabia are due to farming in the northern part of the country for which groundwater and desalinated seawater are used. The results of this study suggest that the main factors affecting the vegetation coverage in the Middle East are governmental policies. These policies can have a positive effect on the vegetation coverage in some countries such as Egypt, Saudi Arabia, Qatar, Kuwait, Iran, and Turkey.

Keywords: Middle East; Moderate Resolution Imaging Spectroradiometer; Normalized Difference Vegetation Index; time series analysis; governmental policy

1. Introduction

During last few decades the impact of global climate change on land-dwelling ecosystems at local, regional, continental, and global scales has triggered public concern and thus additional focus has been given to monitor vegetation growth dynamics [1-8]. Vegetation is simultaneously influenced by the soil characteristics, its moisture and atmospheric parameters [9]. The air temperature and precipitation impacts water balance, and thus the amount of the soil moisture content available for plant growth [10, 11], influencing vegetation dynamics [12]. Natural vegetation is changing not only due to intra-annual seasonal dynamics and inter-annual climate variability, but also other factors, such as anthropogenic activities and/or changes in those activities [13-16]. While field surveys can be used to obtain accurate ground data related to vegetation variations and their indicators; *in situ* observations are expensive, time-consuming, laborious, spatially limited, and are rapidly becoming outdated [17-20]. After the introduction of remote sensing (RS) techniques, satellite-based remotely

sensed data have been progressively used to monitor the vegetation dynamics because of their contiguous long-term spatiotemporal variability, free availability, large geographic coverage, and frequent and near-real-time workability [21-34].

The Moderate Resolution Imaging Spectroradiometer (MODIS) is a spaceborne imaging sensor aboard the NASA Terra satellite, which produces ecological indicators that are available on a global scale [35]. MODIS has a high temporal (daily to annual) and a varying spatial (250 m to 1 km) resolution. The MODIS is used to track environmental characteristics such as land use, food security, environmental sustainability, disruption, and climate change [4]. The vegetation index (VI) is used as an indicator of vegetation variability, and is a sensitive spectral signature of vegetation phenology. It combines different spectral bands of RS data, which can be used to quantify the vegetation conditions [36, 37], growth status, or biophysical variables (e.g., Leaf Area Index LAI, productivity, and vegetation cover types) [38-41]. Among all VIs, the Normalized Difference Vegetation Index (NDVI) is the most well-known and widely used. The NDVI is based on red and near-infrared (NIR) spectra [42, 43]. The NDVI varies from -1.0 to +1.0, where positive values (following an increasing trend) denote healthy vegetation conditions. However, zero and negative values usually indicate non-vegetation elements such as clouds, dust, water, rock, and water vapor [44]. NDVI values close to 0 can also be found in senescent vegetation, in dormancy, or in cultivation sites prepared for sowing or after harvest. The mesophyll structure of healthy leaves influences an NIR spectrum signal, because it strongly imbibes photosynthetically active radiation [10]. The NDVI is used to monitor the green vegetation status and land cover, which comprises unstressed vegetation [23], and to evaluate ecological responses to environmental changes [40, 45, 46]. The NDVI correlates with vegetation functions, such as the biomass [47, 48], primary productivity [49, 50], and LAI, and can be used to investigate land-dwelling vegetation and climate relationships [9, 13-16, 43, 51-54].

The NDVI index has been applied to many scientific studies worldwide. The long-term NDVI can be used to indicate vegetation trends [12, 55, 56] and monitor local, regional, and global trends as well as vegetation diversity [57, 58]. Bagherzadeh et al. confirmed the utility of the NDVI to express the vegetation variability under semiarid climate conditions [12]. In their study NDVI, LU/LC map, and climate variables (temperature, precipitation) were analyzed at both inter-annual and monthly scales, revealing correlations between NDVI variations and yearly sum of the precipitation with correlation coefficient 0.419 and a very high correlation between monthly NDVI variations and air temperature, reaching 0.769 [12]. Therefore, they concluded that the NDVI is a good quantity to investigate vegetation dynamics in the Mashhad-Chenaran plain (northeast of Iran), with relation to climatic parameters in semi-arid ecosystem [12]. The results of several other studies utilizing NDVI time series revealed the recent increase in the vegetation performance in the karst regions [9, 19, 59, 60], indicating that the NDVI of each vegetation type has different value. Evans reported that the viable rainfed agricultural land area has decreased by >170,000 km^2 until the end of the 20th century in the Middle East (ME) due to climate change [61]. Quaye-Ballard et al. showed high variability in the NDVI in the upper east region of Ghana and have found overall negative trend in the vegetation growth during the study period (from 1982 to 2015) [62]. They also recognized anthropogenic activities as a possible reason of 16.6% decrease in vegetation [62]. Zhang et al. studied the spatiotemporal heterogeneity of vegetation coverage with relationship to climate change in the Yangtze river basin (YZRB) and Yellow river basin (YRB) in China and found that the growing-season NDVI increased by 0.011/decade during study period. A significant upward trend in vegetation coverage in the central and eastern part of YRB and the central part of YZRB was found, whereas in the eastern part of YZRB vegetation coverage considerably decreased [63]. They also found in the central area of the YRB-YZRB that the vegetation were influenced more by climate change than by anthropogenic activities, whereas in other parts of YZRB and in the southwest part of the YRB-YZRB areas the vegetation were influenced more by anthropogenic activities than by climate change [63]. Jiang et al. studied the impact of climate change and human activities on vegetation dynamics in the ago-pastoral transitional zone of northern China (APTZNC), an arid and semi-arid ecosystem. In their analysis they combined meteorological data with net primary productivity (NPP) [64]. It stemmed from the analysis of the annual NPP that the vegetation in APTZNC were greener in 48.78%

 doi:10.20944/preprints202010.0208.v2

and degraded only in the 0.39% of the APTZNC area [64]. Greening of the vegetation was caused in 26.93% by climate change, and in 19.80% was due to ecological conservation project [64].

The ME comprises both arid and semiarid regions, which are considered as the hottest places on earth, such as the Saudi Arabia deserts and Dasht-E-Lut in Iran. The vegetation in this region is affected by many anthropogenic and natural phenomena. The region suffers from severe droughts and some of the long-lasting wars (Syria, Yemen, and Iraq). In some parts (e.g. in Egipt) the enormous population pressure exists, causing policy orientation on maximizing food production at the expense of environmental disruptions [65]. Intensively-managed irrigated systems in these areas cause diminishing of water reservoirs [66]. Additionally, traditional agricultural soil management systems increase risks of ground-water pollution, its shortages or salinity buildup [67]. Large parts of ME depend on groundwater raised through wells which are ineffective and costly. In some areas the brackish or salty water is used for agriculture which increases soil salinization. In some mountainous terrains (eg. In Iran or Turkey) extreme variability of air temperatures and wind speed cause cultivation problems as well as water and wind erosion susceptibility [68]. Therefore, in the recent years national policies in ME countries are focused on implementing all possible measures to mitigate desertification processes. Large investments (also with private sector) have been made concerning the control of water in the largest rivers, its preservation and distribution. These efforts brought some progress in reducing the overexploitation of water resources, enabled to increase the non-conventional water sources. Some wealthiest countries managed to create efficient systems of seawater desalinization to improve their irrigation infrastructure and drainage networks [69]. Based on MODIS data Badreldin and Goossens detected anti-desertification change in El-Tina plain and Qanatra Shark in Egipt in the studied years 2002, 2005, 2008 and 2011 and indicated that societal drivers contributed to mitigate and compact desertification process [70]. The same authors analyzed land use/land cover change in El-Arish, Egypt in the period from 1999 to 2010 using multi-temporal Landsat satellite images and noticed a remarkable changes in the vegetation cover as a result anthropogenic activities and the climate impact (mainly wind and water erosion) [11]. In spite of these studies, the knowledge of the vegetation dynamics in the ME is still insufficient. Therefore, the aim of this study was to investigate the trends in vegetation productivity and coverage in the ME using satellite-derived information. An attempt was made to measure the long-term spatiotemporal variability of the vegetation coverage using time series analysis and correlation assessment in ME countries.

2. Materials and Methods

2.1. Study area

The use of "Middle East" first arose in the early years of the present century, referring to the area surrounding the Persian Gulf. According to Fisher, it is the logical intermediate delineation between the Mediterranean "Near East" and "Far East" [71]. The region includes Bahrain, Egypt, Palestine, Iran, Iraq, Israel, Jordan, Kuwait, Lebanon, Oman, Qatar, Saudi Arabia, Syrian, Turkey, the United Arab Emirates (UAE), and Yemen [72, 73]. During the 1990s, the economic development of ME region grew at 50% of the rate of other developing countries [72]. The region is located between 12°N and 42°N and 24°E and 63°E, covering a total area of ~7.2 million km^2 (Figure 1 top panel) and including a population of ~420 million people (Table 1). The largest part of the ground cover is barren land (5,091,844 km^2), whereas the most common vegetation are grasslands (944,286 km^2), croplands (453,315 km^2), and open shrublands (387,244 km^2) (Figure 1, bottom panel & Table 2). It results from Figure 1 that the vegetation occurrence in the studied region is closely related to the orography and the presence of water reservoirs. For example in Iran the vegetation covers mostly the mountain ranges of Zagros and Elburz, whereas in Saudi Arabia and Yemen – the Sarawat mountains. In Egypt influence of the Nile river is clearly visible, and in Iraq - the Euphrates and the Tigris rivers. Unfavorable thermal conditions in the lowlands of the Middle East lead to much lower vegetation cover than in highlands and foreland areas, in which milder weather conditions occur. In Figure 1 the land cover type map from 2017 is presented, whereas the maps for other years are included in the

Preprints (www.preprints.org) | NOT PEER-REVIEWED | Posted: 15 December 2020 doi:10.20944/preprints202010.0208.v2

Supplement 1 file, in Figure S1. For the analyzed years (2001-2019) no significant changes in land cover types were observed.

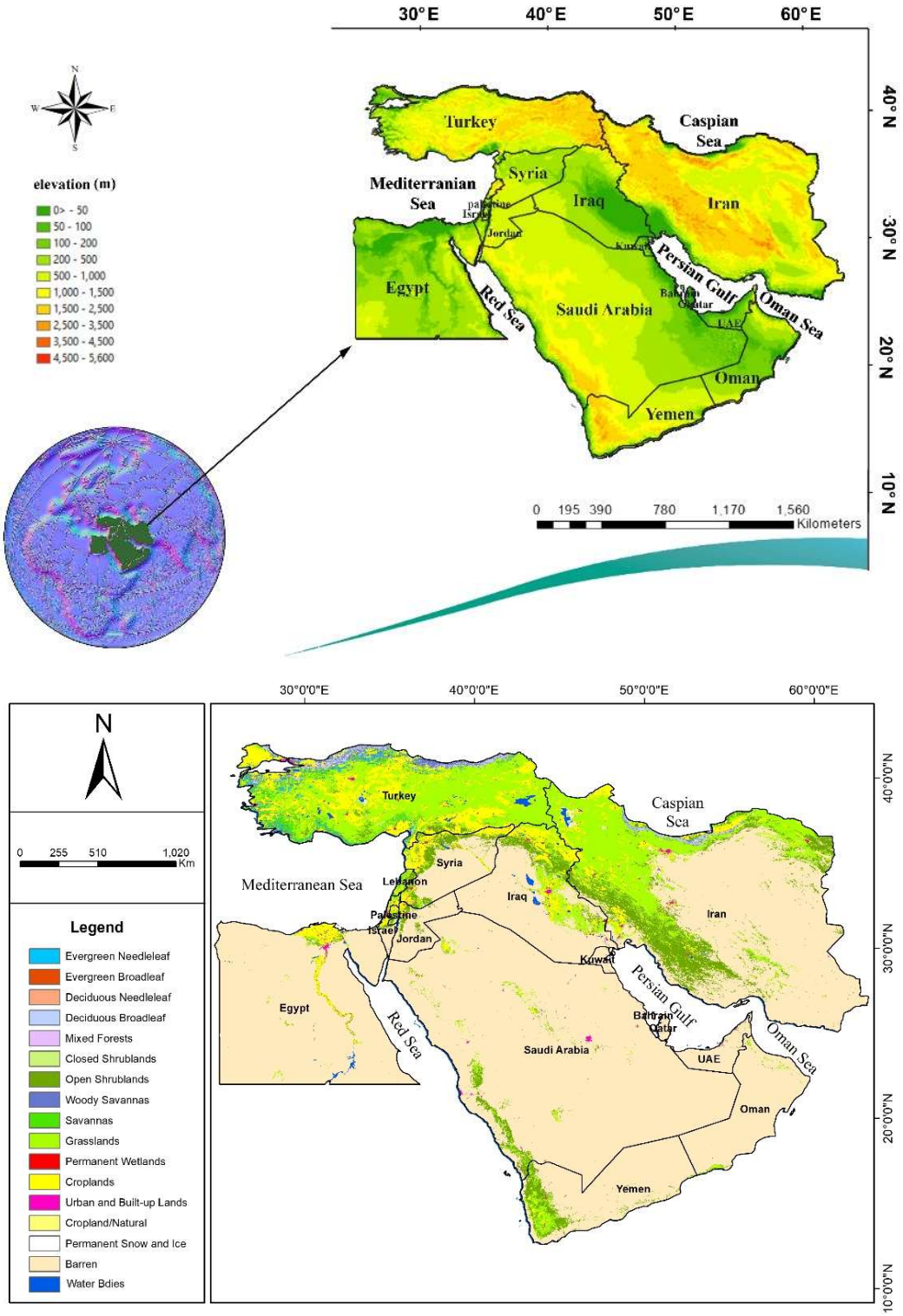

Figure 1. Maps presenting the study area (the Middle East) including an elevation profile (top) and land cover types from MODIS (MCD12Q1) image from 2017 (bottom).

 doi:10.20944/preprints202010.0208.v2

Table 1. Population and area of Middle East countries.

Country name	Middle East population	Population (%)	Area (km²)
Egypt	90,253,760	21.5	1,010,407
Iran	82,467,049	19.6	1,648,195
Turkey	78,214,000	18.6	783,562
Iraq	36,575,000	8.7	438,317
Saudi Arabia	31,521,000	7.6	2,149,690
Yemen	26,745,000	6.4	527,970
Syria	23,270,000	5.5	185,180
Jordan	10,248,069	2.4	92,300
UAE	9,154,000	2.2	82,880
Israel	8,547,000	2.0	20,770
Lebanon	6,185,000	1.5	10,452
Palestine	4,816,503	1.1	6,220
Oman	4,181,000	1.0	212,460
Kuwait	4,161,000	1.0	17,820
Qatar	2,113,000	0.5	11,437
Bahrain	1,781,000	0.4	665
Total	**420,232,381**	**100**	**7,198,325**

Table 2. Land cover types of the Middle East identified from MODIS (MCD12Q1) images using IGBP classification [74, 75].

Land cover type	Area (km²)	Percent of the whole area
evergreen needleleaf forests	20,949	0.29
evergreen broadleaf forests	289	0.005
deciduous needleleaf forests	0	0.0
deciduous broadleaf forests	24,356	0.34
mixed forests	15,105	0.21
closed shrublands	35	0.001
open shrublands	387,244	**5.38**
woody savannas	52,058	0.72
savannas	72,498	1.01
grasslands	944,286	**13.12**
permanent wetlands	5,468	0.08
croplands	453,315	**6.3**
urban and built-up lands	39,784	0.55
cropland/natural vegetation mosaics	8,981	0.12
permanent snow and ice	285	0.004
barren	5,091,844	**70.73**
water bodies	81,827	1.14
Total	**7,198,325**	**100**

 doi:10.20944/preprints202010.0208.v2

2.2. Data description

In this study, we used the Normalized Difference Vegetation Index (NDVI) data acquired by the Moderate Resolution Imaging Spectroradiometer (MODIS), precipitation data from Global Precipitation Measurement (GPM) and Tropical Rainfall Measuring Mission (TRMM) measurements integrated by the Integrated Multi-satellitE Retrievals for GPM (IMERG) algorithm [76, 77], and surface skin temperature and soil moisture content data from NASA Global Land Data Assimilation System (GLDAS) Noah Land Surface Model [78]. To provide an elevation map of the study area the Shuttle Radar Topography Mission (SRTM) digital elevation data with a resolution of 1 arc-second (~30 m) [79] were used, whereas land cover types of the ME were identified using MODIS (MCD12Q1) images, which are produced based on the International Geosphere–Biosphere Programme (IGBP) land cover classification system [80].

2.2.1. NDVI data

The NDVI has become the most common and widely used index to investigate the vegetation status and is derived from the production variety and LAI [81-84]. In the modern era, many scientists used the NDVI in various studies relating to vegetation class, vegetation phenology, continental land cover mapping, chlorophyll content, land use/land cover changes, and water stress [31, 37, 43, 85-89]. The NDVI provides information about the inner mesophyll of healthy green leaves that highly reflects near-infrared (NIR) radiation, whereas leaf chlorophyll and other pigments assimilate a huge proportion of the visible (VIS) radiation. In the case of unhealthy vegetation the spectrum that reflects the inner leaf composition is reversed [24, 81]. The NDVI is calculated as:

$$NDVI = \frac{NIR - RED}{NIR + RED}, \quad (1)$$

where NIR is near-infrared light (at 0.841–0.876 μm) and RED is visible red light (at 0.62–0.67 μm). By definition, the NDVI index ranges from -1 to +1, where healthy vegetation generally falls between values from 0.2 to 0.8 [90-94].

In the present research, the NDVI data were acquired from the Terra-MODIS Vegetation Indices MOD13A1 products delivered by the Earth Observing System of the National Aeronautics and Space Administration (NASA). These products provide the vegetation conditions with a 500-meter spatial resolution and a 16-day temporal resolution (MOD13A1.006__500m_16_days_NDVI). For analysis, the time series of NDVI data from 2001 to 2019 were downloaded using the Application for Extracting and Exploring Analysis Ready Samples (AρρEEARS) application platform (https://lpdaacsvc.cr.usgs.gov.appeears) [95]. The whole downloaded set consisted of 437 images, with 23 images numbered chronologically from 1 to 23 for each year. The quality assessment (QA) was performed for all of the downloaded images using VI quality indicator, which describes the conditions under which each pixel was acquired and/or processed [74]. To obtain the yearly value of the NDVI for each pixel, an arithmetic mean from all of the 23 annual observations was calculated for each pixel as:

$$Yearly\ vegetation\ index = \frac{\sum_{i=1}^{K} NDVI_i}{K}, \quad (2)$$

with $K = 23$. For the seasonal vegetation indices only a subset of the data was used to calculate arithmetic means for each pixel for each year (images with numbers 1-6 for winter, 7-12 for spring, 13-18 for summer and 19-23 for fall vegetation coverage).

Additionally, to study the NDVI variations in more detail and to check what type of the vegetation are increasing/decreasing, the NDVI was divided into seven categories with 0.1 interval (namely < 0.2, 0.2–0.3, 0.3–0.4, 0.4–0.5, 0.5–0.6, 0.6–0.7, 0.7–0.8, and > 0.8) [90-93, 96]. Very low values of NDVI (0.2 and below) correspond to barren areas of rock, sand, or snow, with values between 0.1–0.2 indicating almost absent canopy cover [97]. Moderate NDVI values represent shrubs and grasslands (0.2 to 0.3), sparse vegetation (0.3 to 0.4), and moderate vegetation (0.4 to 0.5). The NDVI values from

 doi:10.20944/preprints202010.0208.v2

0.5 to 0.6 indicate temperate vegetation, 0.6 to 0.7 - dense vegetation, and > 0.7 - very dense vegetation, with values close to +1 (> 0.8) indicating the highest possible density of green leaves [90-93, 96].

To calculate the vegetation coverage, the number of pixels with vegetation, that is, having the NDVI > 0.2, were summed up and multiplied by the resolution of one pixel (500 m x 500 m = 0.25 km^2). The same procedure was used for calculating the yearly and the seasonal vegetation coverages. Additionally, several statistical indicators were calculated using ARC GIS cell statistics. They included seasonal and yearly maximum, average, and majority NDVIs for each ME country and for each year from the period from 2001 to 2019, as well as the average values of these indicators for the whole analyzed period. The majority NDVI is a preferable indicator for studying the variation of the vegetation coverage because other indicators can be sensitive to just one value. For example, the maximum NDVI is sensitive to the highest value; thus, just one value can affect the indicator, whereas the majority refers to the value that occurs most often. Therefore, it is not sensitive to values from one pixel and is representative of the vegetation status in an area. When calculating the statistical measures of the NDVI, only the pixels having NDVI > 0.2 were considered. It was done, because if the areas having NDVI~0.0 (these were covered mostly (~70%) with the barren land) were included to calculation of such measures as the average or majority NDVIs, the final results would be dominated by those values, being very close to 0 and they would practically not change with subsequent years.

2.2.2. Precipitation, surface skin temperature and soil moisture data

The GPM is a result of cooperation between NASA and Japan Aerospace Exploration Agency (JAXA) [98, 99] and is a global successor to TRMM. The GPM was launched in 2014 and its key advancement over TRMM, system developed to observe precipitation in tropical and subtropical regions and launched in 1997, is the extended coverage to higher latitudes (from 65°S to 65°N degrees south over the 35°S to 35°N of TRMM coverage) to provide a near global view of precipitation [100-102]. The GPM is also characterized by an extended capability to measure light rain (< 0.5 $mm \cdot hr^{-1}$), solid precipitation, and the microphysical properties of precipitating particles [102]. The precipitation-related sensors included in TRMM - visible and infrared radiometer system (VIRS), microwave imager (TMI), and precipitation radar (PR) [103, 104] have been substituted in GPM to the first space-borne Ku/Ka-band Dual-frequency Precipitation Radar (DPR) and a multi-channel GPM Microwave Imager (GMI). NASA's TRMM and GPM measurements are now available as one unified data set. In the latest Version 6 release of the Integrated Multi-satellitE Retrievals for GPM (IMERG) early precipitation estimates collected in 2000-2014 during the operation of the TRMM satellite are combined and homogenized with more recent precipitation estimates, collected during operation of the GPM satellite. In this study, the GPM_3IMERGM monthly precipitation dataset with 0.1×0.1 degree spatial resolution and the NASA GLDAS (Global Land Data Assimilation System) surface skin temperature and soil moisture content datasets from the Noah Land Surface Model L4 3-hourly 0.25 x 0.25 degree version 2.1 (V2.1) from 2001 to 2019 were downloaded from Giovanni website (https://giovanni.gsfc.nasa.gov/giovanni/). The temperature data was in Kelvin (K) scale and further converted into Celsius (°C) scale in GIS domain. The unit of downloaded soil moisture data was kg m^{-2} and it was estimated for the 0-10 cm topsoil layer.

2.3. Methods

2.3.1 Anomaly algorithm and interpretation

The anomaly is an indicator calculated on the basis of the selected periods of time and shows how the value of the assessed quantity for a particular time period compares with the entire period [43, 105] by indicating how many standard deviations away a given observation is from the mean. Conceptually, the calculation of the anomaly is equivalent to the calculation of the Z-score used in statistics and is formulated as follows:

$$Zij = \frac{Xij - U}{\sigma ij}, \quad (3)$$

Preprints (www.preprints.org) | NOT PEER-REVIEWED | Posted: 15 December 2020 doi:10.20944/preprints202010.0208.v2

where *Zij* is the anomaly of the *i*-th time period at the *j*-th time-scale, *Xij* is the parameter (as NDVI) sum for the *i-th* time period at the *j*-th time-scale, and *Uij* and *σij* are the long-term mean and standard deviation, respectively, connected with the *i*-th time period at the *j*-th time-scale [106, 107]. A positive anomaly indicates that the values of the investigated quantity are greater than the mean, whereas negative values indicate that the values of the investigated quantity are lower than mean. Typically, data with an anomaly score exceeding an arbitrary threshold of 2 is flagged as abnormal, while data with an anomaly <|0.5| can be treated as typical and is indicated in the figures as "normal area" [108]. In our study, the anomalies were calculated using the time period *i* equal to 1 year, whereas the time-scale *j* was 19 years.

2.3.2 Linear regression

Linear regression is a statistical method to model the relationship by fitting a linear equation between two variables, where one is as an explanatory variable and the other is a dependent variable. In this study, linear regression was used to define the relations of vegetation coverage and precipitation (dependent variables) with time (explanatory variable) at a significance level of 0.05 [109, 110].

3. Results

3.1. NDVI changes

Figure 2 shows the average vegetation coverage (NDVI > 0.2) in the ME during the study period. The vegetation coverage gradually increases from January (12% of the whole study area) and peaks in late April. Consequently, ~21% of the area is covered by vegetation (~1,519,200 km^2). Starting in May, the vegetation cover gradually decreases and reaches its minimum annual value in the warm season by the end of September (14% vegetation coverage; ~1 million km^2). The vegetation cover gradually increases from the first of October to mid-November and, then, decreases. Accordingly, the primary growing season (GS) in the ME starts around January 1 and ends within the first ten days of May (Figure 2). Because the study area is large (extends to different northern latitudes) and the elevation significantly varies, it is difficult to generalize the data for the whole area. Spring is the greenest season. This greenness continues into the summer season until the end of June. Subsequently, the vegetation coverage decreases, primarily because of the scarcity of rain in the study area.

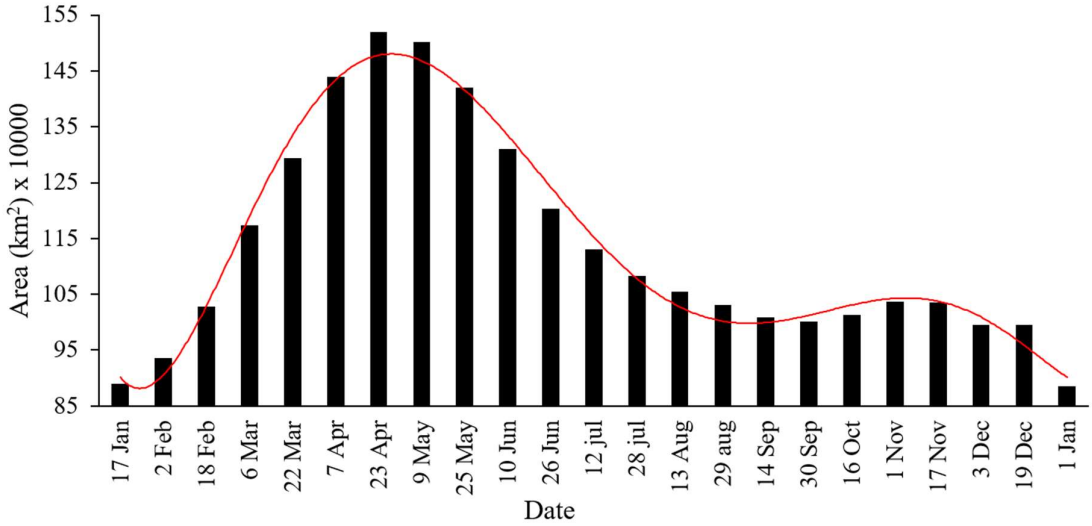

Figure 2. Average annual vegetation coverage in the Middle East during 2001–2019.

Preprints (www.preprints.org) | NOT PEER-REVIEWED | Posted: 15 December 2020 doi:10.20944/preprints202010.0208.v2

Figure 3 shows the annual average vegetation coverage in the ME based on all NDVI categories (0.2–0.3, 0.3–0.4, 0.4–0.5, 0.5–0.6, 0.6–0.7, 0.7–0.8, and > 0.8) for the study period. A significant positive trend of the NDVI coverage in the study area can be observed in the period 2001–2019 (R = 0.75, p-value = 0.05); however, a substantial interannual variability can also be detected. The years 2015, 2018, and 2019 exhibit the maximum coverage, accounting for 17%, 18%, and 20% of the study area, respectively (1.22, 1.28, and 1.43 million km², respectively), whereas the minimum vegetation coverage was observed in 2001, 2003, and 2008, accounting for 14%, 15%, and 14% of the study area, respectively (1.02, 1.05, and 0.975 million km², respectively).

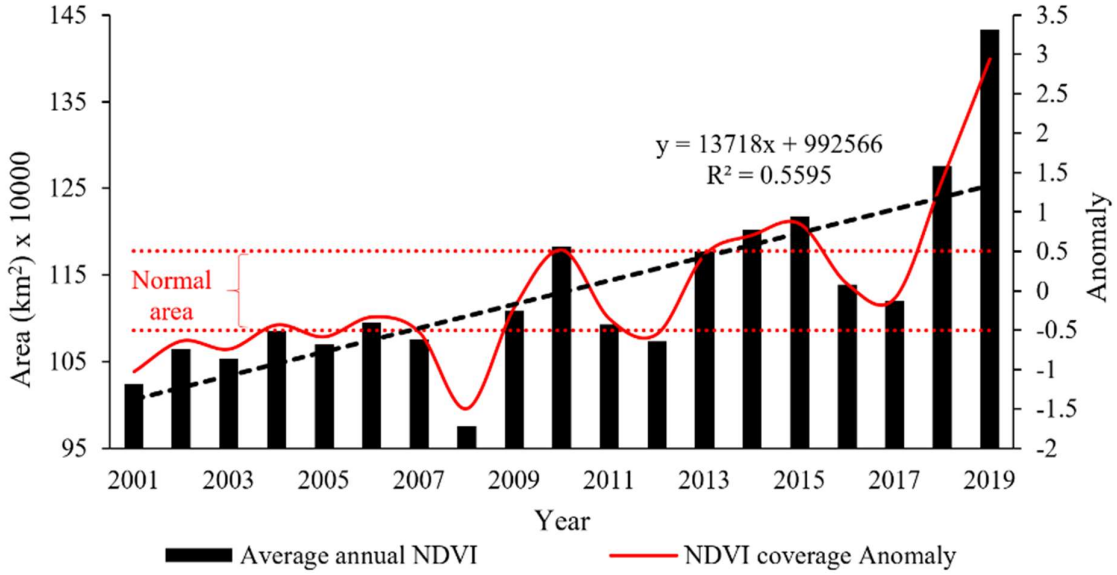

Figure 3. Average annual vegetation coverage in the Middle East during 2001–2019 (black bars), showing the linear trend line (black discontinuous line) supplemented by the Normalized Difference Vegetation Index (NDVI) coverage anomaly (red continuous line) and normal area (red dotted lines).

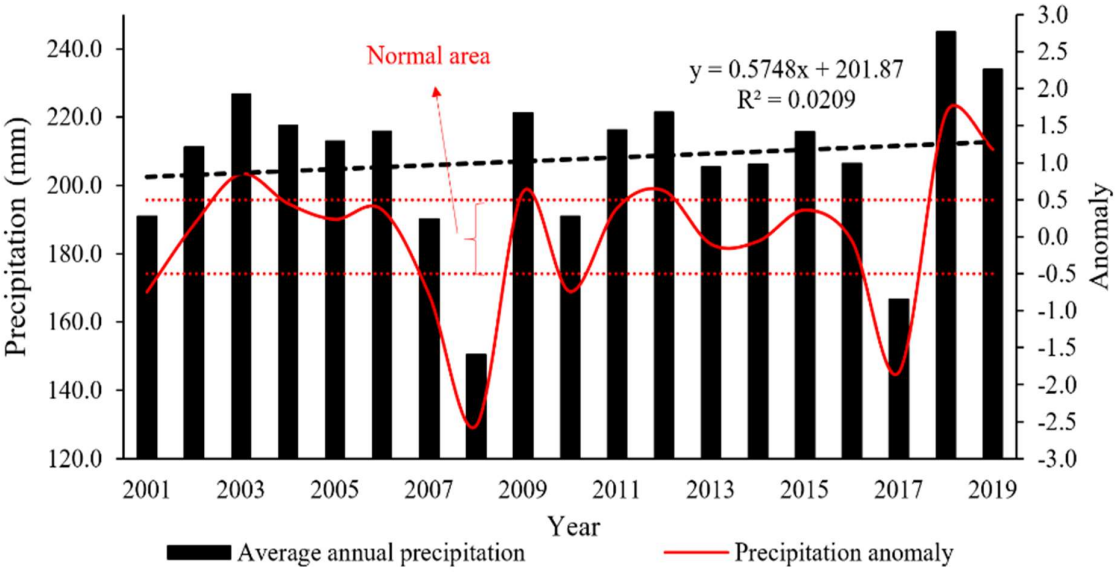

Figure 4. Total annual precipitation in the Middle East during 2001–2019 (black bars), with the linear trend line (black discontinuous line), precipitation anomaly (red continuous line), and normal area (red dotted lines).

Preprints (www.preprints.org) | NOT PEER-REVIEWED | Posted: 15 December 2020 doi:10.20944/preprints202010.0208.v2

Figure 4 shows the changes in the total annual precipitation in the ME during the study period. The trend line indicates that the precipitation insignificantly changes during the study period. Instead, a high interannual variability can be observed, which correlates with the interannual variability of the NDVI (Figure 5). This suggests that precipitation is one of the factors affecting the changes in the NDVI; however, it cannot fully explain the significant positive trend of the NDVI shown in Figure 3. In fact, positive and significant correlation between the annual anomaly of precipitation and vegetation coverage was obtained (R = 0.5). However, a factor that influenced vegetation coverage much more strongly was the surface skin temperature (R = 0.73). The correlation between soil moisture and vegetation coverage was very small and insignificant (Table 3).

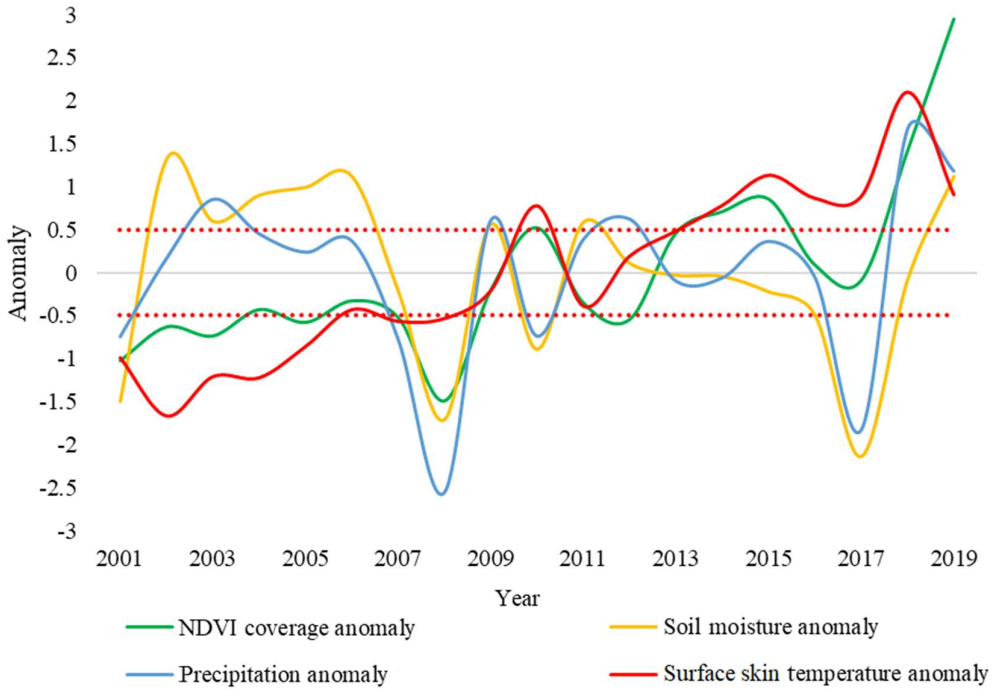

Figure 5. The annual anomaly of soil moisture, precipitation, vegetation coverage and surface skin temperature in the Middle East during 2001–2019.

Table 3. The correlation coefficients R between annual anomaly of soil moisture, precipitation, vegetation coverage and surface skin temperature in the Middle East during 2001–2019.

Anomaly of	NDVI coverage	Soil Moisture	Precipitation	Surface skin temperature
NDVI coverage	1			
Soil Moisture	0.21	1		
Precipitation	**0.50***	**0.77***	1	
Surface skin temperature	**0.73***	-0.31	0.16	1

* denotes correlations significant at p=0.05

Figure 6 shows the maps of the NDVI in the study area for four years (2003, 2009, 2013, and 2019). A large increase in the vegetation area can be observed on the border of Iran and Iraq, Iraq, and Saudi Arabia, and Israel, Lebanon, and Jordan; in the central part of Turkey; in the northern part of Syria; and in the western parts of Saudi Arabia and Yemen.

Preprints (www.preprints.org) | NOT PEER-REVIEWED | Posted: 15 December 2020 doi:10.20944/preprints202010.0208.v2

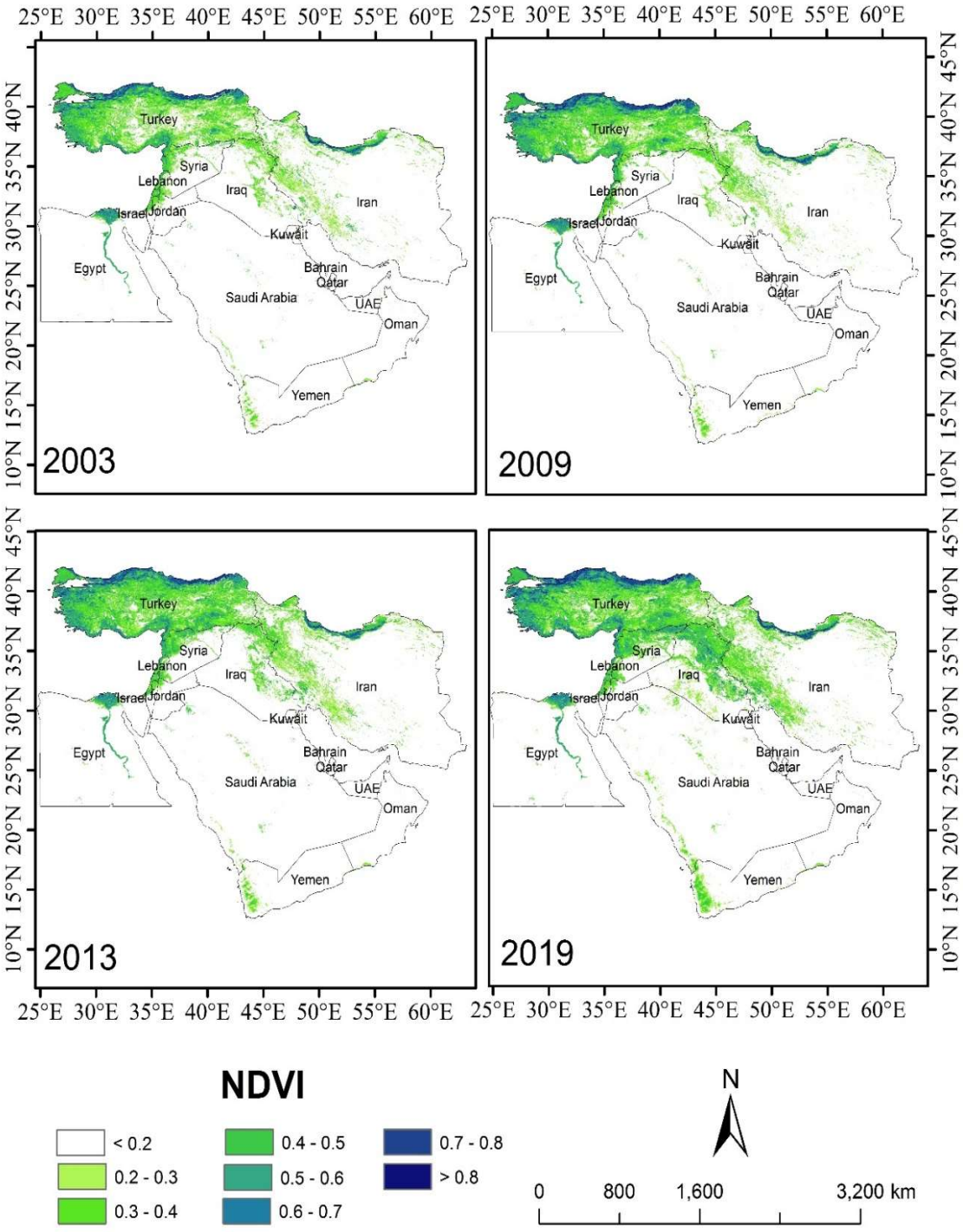

Figure 6. Maps of the Normalized Difference Vegetation Index (NDVI) for the study area for the chosen years (2003, 2009, 2013, and 2019).

Figure 7 shows the time series of different NDVI categories for the ME from 2001 to 2019. A significant increasing linear trend (p-value = 0.05) can be observed in the NDVI all categories above 0.3 and an insignificant increase can be detected in the NDVI category 0.2–0.3. In all categories, a trough can be observed in 2008, 2012, and 2017 and a ridge can be detected in 2010, 2015, 2018, and 2019. This indicates that the first group is the driest (less vegetation) and the second group is the greenest (denser vegetation) during the study period (Figure 7).

Preprints (www.preprints.org) | NOT PEER-REVIEWED | Posted: 15 December 2020 doi:10.20944/preprints202010.0208.v2

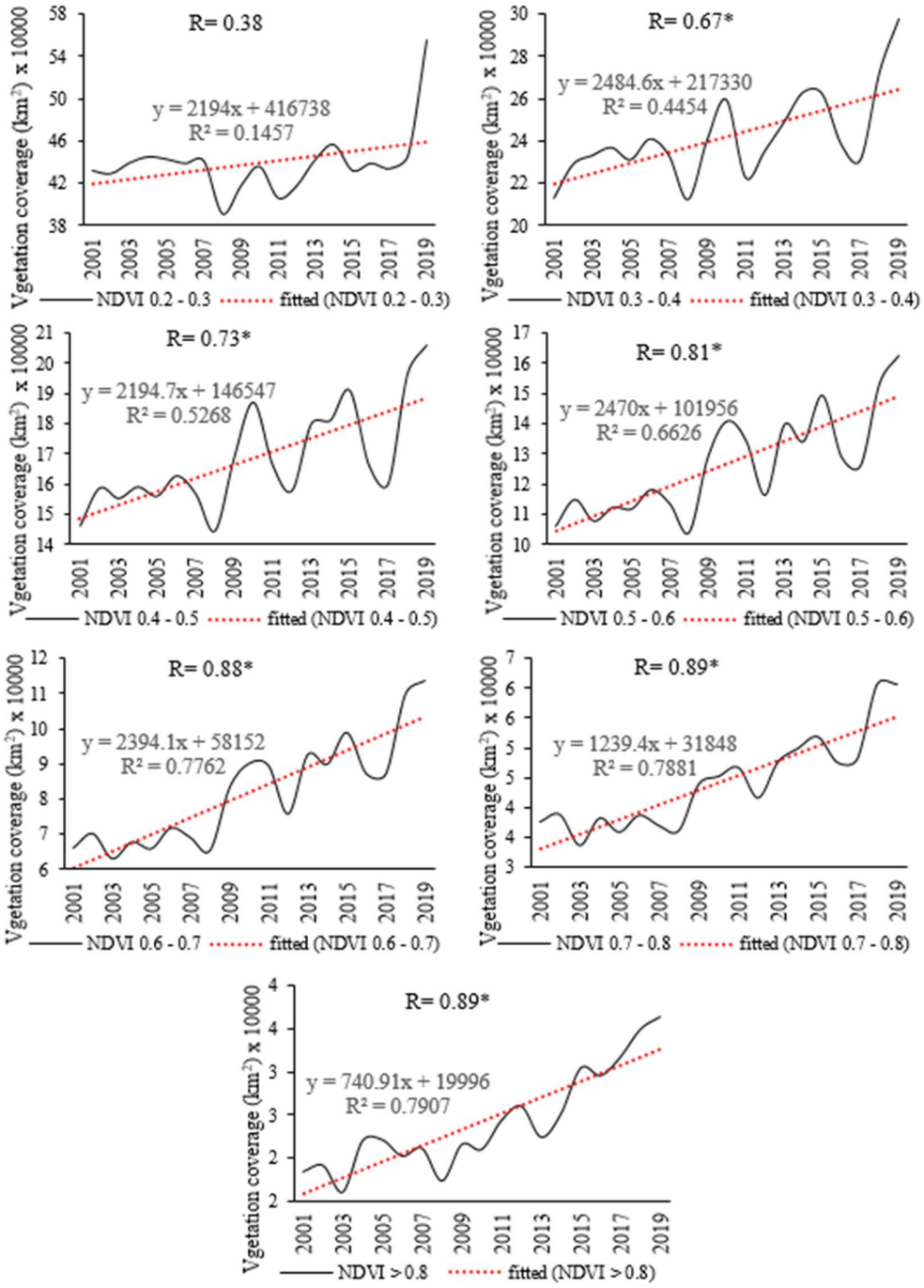

Figure 7. Average annual coverage (km²) for different vegetation categories in the Middle East during 2001–2019. *denotes that the trend is significant at p = 0.05.

Table 4 presents the correlation coefficients of NDVI over time in the ME for time series of 16-day MODIS images, having fixed date from subsequent years during the study period. A significant positive linear trend can be observed in all images, except for the images obtained on January 17, February 2, and March 6. This reveals that the ME is becoming greener and the vegetation coverage increases in all months. The correlation coefficients obtained for August 13 and 29 and September 14 and 30 are higher than those determined in other months (R = 0.76, 0.76, 0.81, and 0.83, respectively).

 doi:10.20944/preprints202010.0208.v2

Table 4. Correlation coefficients for the time series of vegetation coverage determined from MODIS images having fixed dates from subsequent years for the Middle East for the period 2001–2019.

Date	Correlation
1 Jan	0.59*
17 Jan	0.35
2 Feb	0.41
18 Feb	0.48*
6 Mar	0.40
22 Mar	0.46*
7 Apr	0.57*
23 Apr	0.60*
9 May	0.62*
25 May	0.57*
10 Jun	0.56*
26 Jun	0.65*
12 Jul	0.67*
28 Jul	0.73*
13 Aug	0.76*
29 Aug	0.76*
14 Sep	0.81*
30 Sep	0.83*
16 Oct	0.69*
1 Nov	0.66*
17 Nov	0.67*
3 Dec	0.62*
19 Dec	0.62*

* denotes a significant correlation at $p = 0.05$.

3.2. *Seasonal NDVI dynamics*

Figures 8 and 9 show the seasonal NDVI dynamics of the ME in the study period (2001–2019). Overall, vegetation covers ~19.2% of the study area during the study period. In the study area, spring is the greenest season, followed by winter, fall, and summer, with vegetation coverage of 22.8%, 20.2%, 17%, and 16.8% of the study area, respectively. In all seasons, the densest vegetation coverage was observed in the coastal areas of the Caspian Sea in northern Iran, Black Sea in northern Turkey, Mediterranean Sea in western and southwestern Turkey, western Syria, Lebanon, Israel, Palestine, and Egypt or along large rivers such as the Nile. The driest countries in the ME are Qatar, Kuwait, the UAE, and Saudi Arabia, with vegetation coverage accounting for less than 1% of the total area of the country. Oman, Bahrain, Egypt, Jordan, and Yemen have vegetation coverage of 1%, 2.7%, 3.7%, 3.9%, and 4.3% of the whole ME, respectively (Figures 8–9 and Table 5).

Preprints (www.preprints.org) | NOT PEER-REVIEWED | Posted: 15 December 2020 doi:10.20944/preprints202010.0208.v2

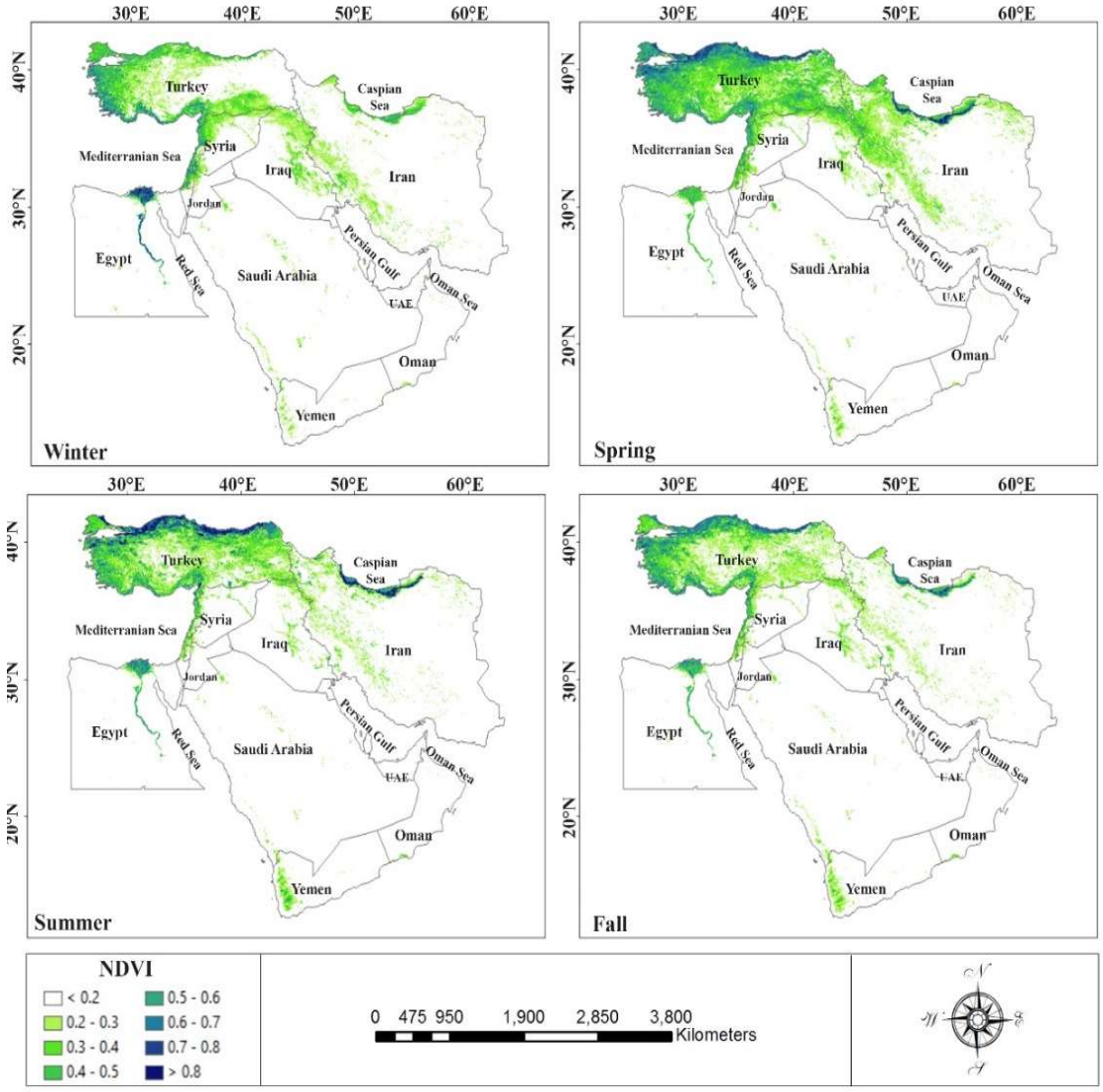

Figure 8. Average seasonal Normalized Difference Vegetation Index (NDVI) in the Middle East for the period 2001–2019.

Figure 9 shows the average seasonal vegetation coverage percentage, surface skin temperature and precipitation for each country in the ME. In winter, Palestine, Lebanon, and Turkey are the greenest countries in the study area, with vegetation coverage of 76.9%, 67.6%, and 54.2%, respectively. The highest precipitation was recorded during the winter (reaching 269, 400, and 254 mm in Palestine, Lebanon, and Turkey, respectively). In spring, Turkey, Lebanon, and Palestine were the greenest countries, with vegetation coverage of 93.8%, 77.7%, and 67.2%, respectively. In summer and fall, Turkey, Lebanon, and Palestine were the greenest, with vegetation coverage of 83.4%, 66.1%, and 39.9% in summer and 73.7%, 66%, and 47.7% in fall, respectively. In spring, summer, and fall, the highest values of the precipitation were recorded in Turkey and Yemen (between 58 and 86 mm). The skin surface temperature varied significantly depending on the season, but was highest in UAE, Oman, Quatar, Kuwait, Saudi Arabia and Yemen (> 28°C in the spring and > 34°C in the summer). Egypt, Kuwait, Jordan, Qatar, UAE, and Saudi Arabia were the driest countries (< 8 mm in spring and < 5 mm in summer). In all seasons, Qatar, UAE, Saudi Arabia, Kuwait, and Oman were the least vegetated, with vegetation coverage <1.2% (Figures 8–9 and Table 5).

Preprints (www.preprints.org) | NOT PEER-REVIEWED | Posted: 15 December 2020 doi:10.20944/preprints202010.0208.v2

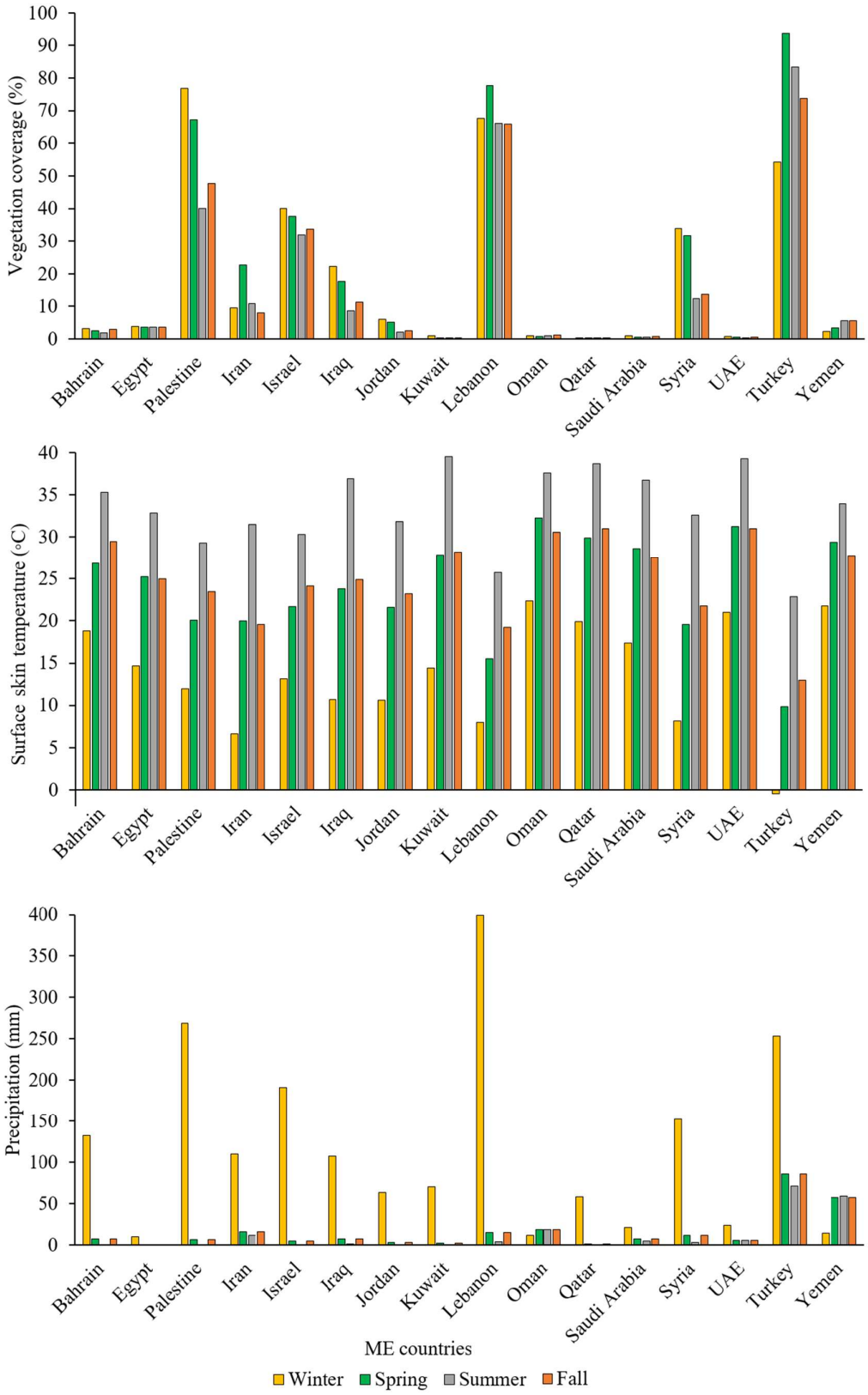

Figure 9. Average seasonal: vegetation coverage percentage, surface skin temperature and precipitation for the period 2001–2019 for each country of the Middle East.

 doi:10.20944/preprints202010.0208.v2

Table 5. Average seasonal vegetation coverage percentage in Middle East countries for the period 2001–2019.

Country	Winter (%)	Spring (%)	Summer (%)	Fall (%)	Average (%)
Bahrain	3.2	2.6	1.9	3.0	2.7
Egypt	3.8	3.6	3.6	3.6	3.7
Palestine	76.9	67.2	39.9	47.7	57.9
Iran	9.5	22.6	10.9	8.0	12.7
Israel	40.0	37.6	31.8	33.6	35.7
Iraq	22.2	17.7	8.8	11.3	15.0
Jordan	6.0	5.1	2.0	2.6	3.9
Kuwait	1.0	0.1	0.1	0.4	0.4
Lebanon	67.6	77.7	66.1	66.0	69.3
Oman	1.0	0.8	1.0	1.2	1.0
Qatar	0.3	0.1	0.1	0.2	0.2
Saudi Arabia	1.0	0.6	0.5	0.8	0.7
Syria	33.9	31.6	12.5	13.7	22.9
UAE	0.8	0.5	0.2	0.5	0.5
Turkey	54.2	93.8	83.4	73.7	76.3
Yemen	2.4	3.5	5.6	5.6	4.3
Average (%)	**20.2**	**22.8**	**16.8**	**17.0**	**19.2**

Figure 10 shows the seasonal average and maximum NDVI of the ME countries from 2001 to 2019. In winter, the maximum NDVI in Egypt, Turkey, and Israel is 0.84, 0.81, and 0.76, respectively, and the NDVI average in Egypt, Israel, and Lebanon is 0.58, 0.48, and 0.41, respectively. The maximum NDVI is the lowest in Bahrain, Oman, and UAE (0.39, 0.53, and 0.55, respectively) and the average NDVI is the lowest in UAE, Bahrain, and Yemen (0.24, 0.246, and 0.249, respectively). In spring, the NDVI is the highest in Iran, Turkey, and Syria (0.86, 0.85, and 0.77, respectively) and the highest NDVI average in Turkey, Egypt, and Lebanon is 0.43, 0.404, and 0.402, respectively. The lowest maximum NDVI was observed in Bahrain, Oman, and Qatar (0.35, 0.43, and 0.43, respectively) and the lowest average NDVI of 0.231, 0.233, and 0.25 were detected in UAE, Bahrain, and Oman, respectively. In summer, the NDVI the highest in Turkey, Iran, and Syria (0.92, 0.88, and 0.79, respectively) and the highest NDVI average in Egypt, Turkey, and Iran is 0.49, 0.41, and 0.34, respectively. Moreover, the lowest maximum NDVI was observed in Bahrain, Qatar, and Kuwait (0.33, 0.38, and 0.42, respectively) and the lowest average NDVI was detected in Bahrain, UAE, and Palestine (0.227, 0.229, and 0.24, respectively). In fall, the maximum NDVI was observed in Turkey, Iran, and Egypt (0.84, 0.82, and 0.76, respectively) and the highest NDVI average in Egypt, Turkey, and Lebanon is 0.45, 0.38, and 0.37, respectively. The lowest maximum NDVI was observed in Bahrain, Kuwait, and Qatar (0.37, 0.48, and 0.49, respectively) and the lowest average NDVI was detected in Bahrain, UAE, and Kuwait (0.23, 0.24, and 0.25, respectively).

Preprints (www.preprints.org) | NOT PEER-REVIEWED | Posted: 15 December 2020 doi:10.20944/preprints202010.0208.v2

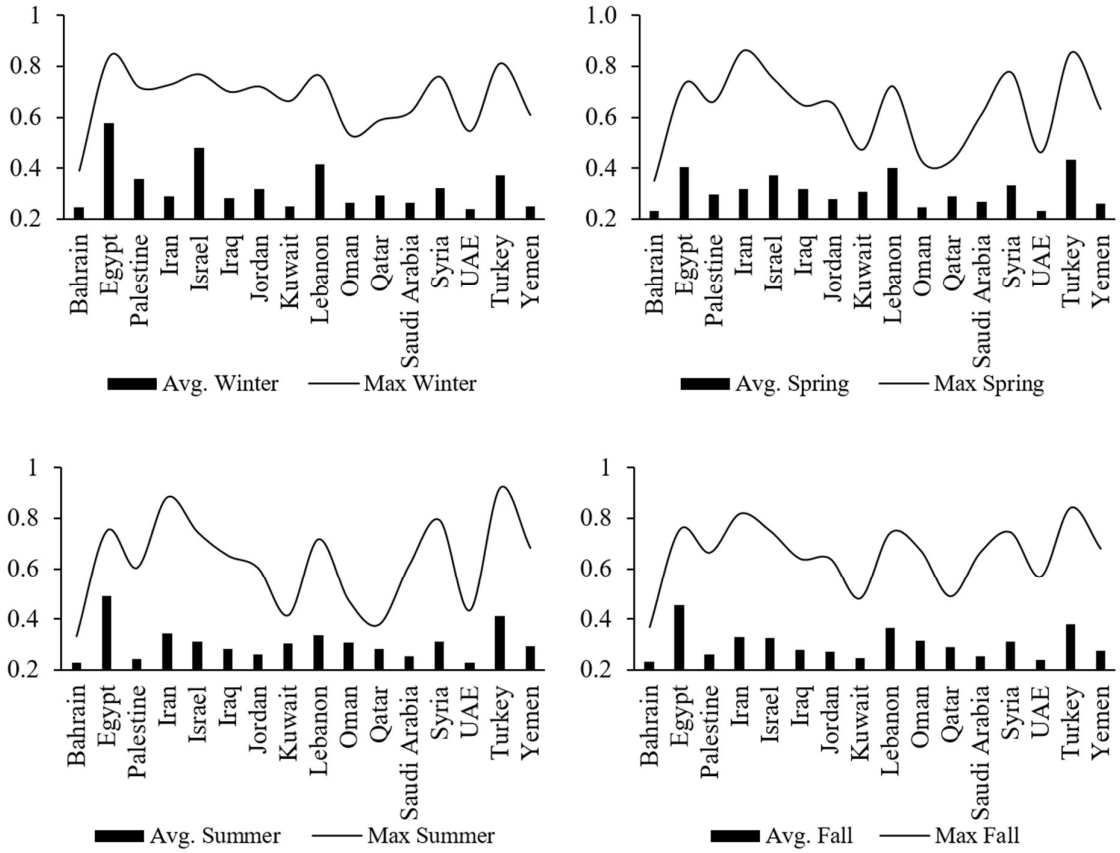

Figure 10. Seasonal average and seasonal maximum Normalized Difference Vegetation Index (NDVI) for each country in the Middle East during 2001–1019.

3.3. Yearly NDVI dynamics

Table 6 shows the correlation coefficients of the annual coverage, and the maximum, average, and majority NDVI over time for each country in the ME, calculated for the period from 2001 to 2019. From 2001 to 2019, the annual coverage significantly increases in Egypt, Iran, Iraq, Kuwait, Lebanon, Oman, Qatar, Saudi Arabia, Turkey, and Yemen. A significant negative NDVI trend was observed in the UAE ($R = -0.72$, p-value = 0.05). The trends determined for Bahrain, Palestine, Israel, Jordan, and Syria are insignificant. Overall, the annual coverage in the ME shows a significant positive trend ($R = 0.47$, p-value = 0.05) from 2001 to 2019. In Egypt and Qatar, the annual coverage continuously increases, with the strongest positive trend in the ME ($R = 0.99, 0.91$, $p = 0.05$). Table 6 shows that the vegetation coverage in the UAE decreases from 2001 to 2019.

The maximum NDVI in the ME exhibits a significant positive trend in Bahrain, Palestine, Kuwait, Lebanon, Saudi Arabia, Turkey, and Yemen. An insignificant positive trend can be observed for Egypt, Iran, Israel, Iraq, Jordan, Qatar, Syria, and the UAE. A significant negative trend was detected for Oman ($R = -0.47$, p-value = 0.05). The strongest correlations were observed in Palestine and Lebanon, with $R = 0.90$ and 0.88, respectively, and a p-value of 0.05. The overall trend of the maximum NDVI in the ME is positive and marginal ($R = 0.43$, $p = 0.05$).

The average NDVI in ME countries exhibits a significant positive trend in Palestine, Iraq, Lebanon, Saudi Arabia, UAE, Turkey, and Yemen. The strongest correlations were observed in Turkey and Saudi Arabia ($R = 0.88$ and 0.83, respectively, and $p = 0.05$). In addition, a significant negative trend was observed in Egypt, Kuwait, and Qatar, with $R = -0.77, -0.65$, and -0.64, respectively, and a p-value of 0.05. In Oman and Saudi Arabia, the average NDVI shows no trend during the study period.

 doi:10.20944/preprints202010.0208.v2

Table 6. Correlation coefficients of NDVI factors in the Middle East for the period 2001–2019.

Country	Annual coverage	Max NDVI	Average NDVI	Majority NDVI
Bahrain	0.37	0.69*	-0.27	-0.36
Egypt	0.99*	0.37	-0.77*	0.04
Palestine	0.16	0.90*	0.47*	0.31
Iran	0.68*	0.44	-0.39	0.11
Israel	0.16	0.26	0.40	0.26
Iraq	0.49*	0.26	0.75*	-0.35
Jordan	0.16	0.36	0.27	-0.09
Kuwait	0.71*	0.58*	-0.65*	-0.19
Lebanon	0.63*	0.88*	0.56*	-0.08
Oman	0.54*	-0.47*	0.01	-0.23
Qatar	0.91*	0.28	-0.64*	-0.20
Saudi Arabia	0.83*	0.71*	0.83*	-0.03
Syria	0.18	0.13	0.12	0.18
UAE	-0.72*	0.36	0.64*	-0.31
Turkey	0.75*	0.64*	0.88*	0.54*
Yemen	0.63*	0.50*	0.76*	-0.07
Average	**0.47***	**0.43**	**0.19**	**-0.03**

* denotes that the correlation is significant at p = 0.05;
NDVI: Normalized Difference Vegetation Index

The majority NDVI in Turkey exhibits a significant positive trend (R = 0.54, p-value = 0.05); in other ME countries, the trend is insignificant. An insignificant positive trend was observed in Bahrain, Iraq, Kuwait, Oman, Qatar, and the UAE; in Bahrain, Iraq, and the UAE, the correlation is stronger than in other countries (R = -0.36, -0.35, and 0.31, respectively). An insignificant positive trend was observed in Palestine, Iran, Israel, and Syria; in Palestine and Israel, this correlation is stronger than in other countries (R = 0.31 and 0.26) during 2001–2019.

4. Discussion

Water scarcity is one of the most severe issues in the ME. It can directly affect the vegetation coverage in this area. Water scarcity has several reasons including high temperatures, relatively irregular dissemination of rainfall, increasing irrigation water loads, and tourism inflation [111, 112]. Furthermore, climate change likely augments this situation. With respect to long-term trends of vegetation coverage and productivity, government policies play vital roles in this arid and semiarid region. The greenest areas of the region are located in 1) mountainous areas and 2) coastal areas of the Black, Caspian, and Mediterranean seas. The water bodies in the southern regions of the ME do not have any effect on the increasing vegetation coverage and the role of mountainous areas (elevation) is more important than the distance to the water bodies in these regions of the study area. Therefore, three main elements affect the vegetation cover in the study area: 1) elevation; 2) distance from the waterbodies in the western and northern regions; and 3) geographical coordinates (latitudes).

The main weather phenomenon in the Persian Gulf, Oman Sea, Indian Ocean, Arab Sea, and the Red Sea is Subtropical High Pressure (STHP). This phenomenon prevents any convectional flows and there is no dense vegetation in the coastal areas of the mentioned water bodies despite the high humidity. The study area comprises the driest deserts in the world due to the STHP. The region is

 doi:10.20944/preprints202010.0208.v2

characterized by very scarce vegetation, which entirely depends on the existence of the mountainous area [113-116]. The northern and western parts of the study area are located in the pathway of the westerlies (anti-trades, that is, steady prevailing winds that blow from the west toward the east and overlie the trade winds) [117, 118]. The main factors affecting the atmospheric dynamics are westerlies and the large water bodies (Black, Mediterranean, and Caspian seas), which supply the water vapor; therefore, these areas contain the densest vegetation in the ME [119-122].

In Egypt, almost all green places are located in the Nile Delta and along the Nile River, while other parts of the country (~97%) are characterized by the desert. The annual vegetation coverage of this country shows the strongest positive trend in the ME ($R = 0.99$, p-value = 0.05). Kuwait and Qatar have similar but weaker trends. The one of the main reasons for this strong positive trend in Egypt are governmental policies, which aim to extend the forest area of the country. Recently, 155,500 feddan (1 feddan = 4,200 m2) that is equal to 653 km^2 of wood forests and bio-oil crops have been irrigated with TWW (Treated WasteWater) in the desert areas adjacent to wastewater treatment plants. The Serapium Forest (located in the Ismailia governorate) is an example of the successful TWW use in Egypt. Various species of woody trees were well-adapted to the arid environment and provided a high wood yield in Serapium [123]. Also, scientists are recuperating wastewater from the city of Ismailia in northern Egypt and are using water to produce fecundate trees. Within less than 20 years, over 4000 km^2 of forests and other vegetation were developed in the desert, which is the main reason for the increase in the annual vegetation coverage in Egypt from 2001 to 2019, which is consistent with findings of other scientists [123-125].

Despite the increase in the annual vegetation coverage in Egypt during the study period, the average NDVI is decreasing ($R = -0.77$, p-value = 0.05). This is due to the creation of new forest areas by policymakers, which leads to an increase in the annual coverage. The leaf cover of these new forest areas is still low, resulting in low NDVI, and this is the main reason why a decrease in the average NDVI is observed. However, this trend cannot be generalized to other countries. For example, a significant increase both in the annual vegetation coverage and the monthly average NDVI can be observed in Iraq, which includes areas with very sparse vegetation. The monthly average NDVI in this country is ~0.27 in all seasons and winter is the greenest season. Therefore, when local governments or farmers start to work on bare land, the average NDVI increases [126].

Turkey is the only country in the ME in which all NDVI indicators are significant and increasing. Both the vegetation coverage and density (expressed by significant and positive trend of the maximum, average, and majority NDVI) increased from 2001 to 2019 in this country. The main reason is the construction of some of the biggest dams in the ME, such as the Atatürk Dam (1995) and Ilisu Dam (2006), which supported the increase in the vegetation coverage in these regions. Ilisu Dam is part of Turkey's large-scale project known as GAP (Guneydogu Anadolu Projesi) or the Southeastern Anatolia Project that involves the construction of 22 dams on the Euphrates and Tigris, as well as 19 hydropower stations. Approximately one-fifth of the Turkish total irrigated lands and one-third of the energy potential of Turkey are located in this region [127]. Our results are consistent with the findings of Özcan et al. [128]. Due to the inundation of the Atatürk Dam Lake, a large area of agricultural fields (~368 km^2) has been affected. However, the agricultural fields in the Harran Plain increased by 56.3% (by 1552 km^2 up to 2756 km^2) because of irrigation during the period 1984–2011 [128].

A major concern for Syria, Iran and Iraq countries in not only Atatürk Dam or Ilisu Dam having 10 billion m^3 of capacity, but the entire Turkish multi-dam project. The volume of the reservoirs created by Turkish dams built within GAP project on the sources of the Tigris and Euphrates is 120 billion cubic meters, while the annual flow of these two rivers is 47 billion cubic meters [127, 129, 130]. The Ilisu Dam, built upstream from the existing Mosul Dam in Iraq, has drained most of the Mosul Dam catchment area. The originally planned Mosul Dam watershed (with area of 54,900 km^2) has been reduced to about one-fifth of the total area [129, 130]. The negative effect of the Turkish dams construction on the vegetation of Syria and Iraq is visible in Figure 11, presenting selected parts of the maps from Figure 6 to highlight the details. The vanishing of the vegetation (change in the NDVI from the values from the range 0.3-0.6 to NDVI < 0.2) is clearly noticeable in Syria and Iraq

Preprints (www.preprints.org) | NOT PEER-REVIEWED | Posted: 15 December 2020 doi:10.20944/preprints202010.0208.v2

south of the Turkish between the 2003 and 2006. To counteract the negative effect of Turkish dams built within GAP project, Syria, Iran and Iraq have constructed their dams (e.g. Karun 3 in 2005 and Karun 4 in 2010 in Iran with total capacity of 5.1 billion m^3 and Darbandikhan Dam in 2013 in Iraq with total capacity of 3 billion m^3), which resulted in greening of the areas of Syria, Iran and Iraq located in Tigris–Euphrates river basin. The water availability for agricultural production were also improved as a result of coordinated common policies of neighboring countries, which signed a political agreements (Water Laws) concerning important aspects of water management [131].

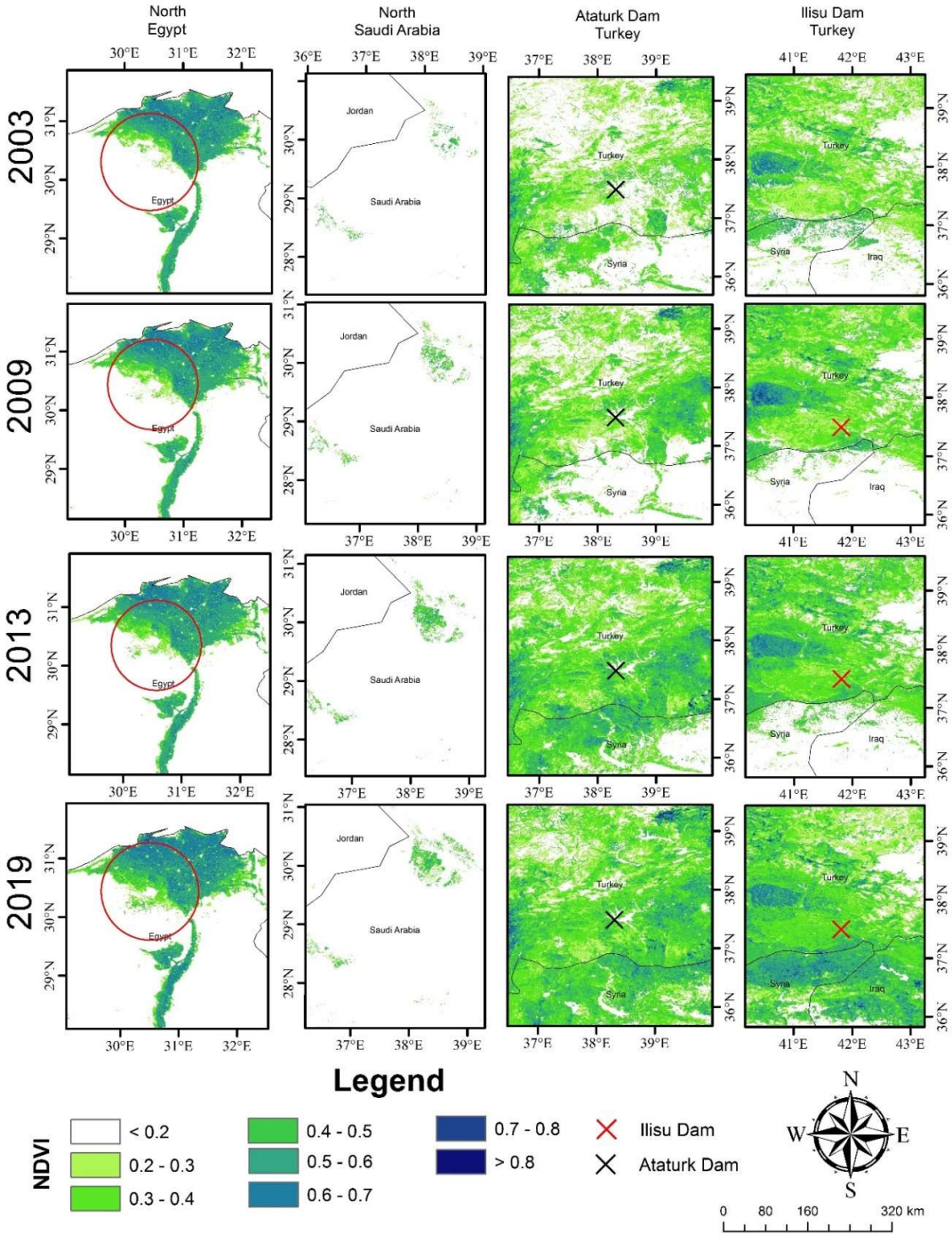

Figure 11. Maps of the NDVI for the selected years (2003, 2009, 2013, and 2019) and areas (south-west part of Nile Delta in northern Egypt, northern Saudi Arabia, and region surrounding the Atatürk and Ilisu dams in southern Turkey) reflecting the progressive impact of anthropopressure.

 doi:10.20944/preprints202010.0208.v2

Because water resources are low and the average annual precipitation is below 100 mm, Saudi Arabia has become the world's poorest country in terms of water. Groundwater, surface water, desalinated seawater, and treated wastewater are the major sources of drinking water [132]. However, during 2001–2019, the annual vegetation coverage and maximum and average NDVI significantly increased in the country. This is due to the significant amount of farming in the northern parts of the country. The farming areas and greenhouses are irrigated using groundwater, and some of them are using desalinated seawater [133].

UAE is a small country in a large desert. During the study period, the annual coverage of this country significantly decreased compared with that of all other countries in the ME; however, the average NDVI significantly increased. Therefore, it can be concluded that very sparse vegetation vanished during the study period. Almost all remaining vegetation near the inhabited areas has been protected and improved, and the average NDVI significantly increased during 2001–2019.

The increase in the NDVI in the above-mentioned countries can be attributed to anthropopressure and is illustrated in Figure 11. A rapid growth in NDVI can be observed in areas where government policies regarding the irrigation of agricultural fields were established. These policies either include the use of desalinated seawater or groundwater (Nile Delta in northern Egypt or northern Saudi Arabia) or water from lakes that were created by dam construction (Atatürk and Ilisu dams in southern Turkey, Karun 3 and Karun 4 in Iran, or Darbandikhan Dam in Iraq).

5. Conclusions

In this study, the interannual and interseasonal variabilities of the vegetation in the ME were analyzed. The results show that climate inconsistency and drought are common phenomena in the entire region. Areas with steep precipitation gradients and marginal rain-fed agricultural fields are the main areas of interest with respect to the mitigation of drought based on the development of local processes to assess, monitor, and evaluate the vegetation dynamics.

The results reveal that the NDVI in the ME increases from January to late April, indicating that ~21% of the area is covered by vegetation. Starting in May, the vegetation cover decreases and the minimum annual coverage (14%) is reached in the warm season by the end of September. Therefore, it can be concluded that the main GS in the ME starts around January 1 and ends within the first ten days of May.

During the study period, the NDVI coverage exhibited a significant positive trend in the study area, with a significant increase in all of the assumed NDVI categories above the NDVI 0.3. The vegetation coverage shows a positive increasing trend in all months. Spring is the greenest season, followed by winter, fall, and summer. Vegetation covers ~19.2% of the whole study area. All of this suggests, that the ME is becoming greener in the analyzed period.

The densest vegetation coverage can be observed in the coastal areas of the Caspian, Black, and Mediterranean seas and along the large rivers. The driest countries in the ME are Qatar, Kuwait, the UAE, and Saudi Arabia.

The main factors affecting the vegetation coverage in the ME, except from meteorological variables, are government policies. These policies can have a positive and continuous effect on the vegetation coverage, as observed in Egypt, Saudi Arabia, Qatar, Kuwait, Iran, and Turkey. However, some of these policies can have negative effects on other countries. For example, the construction of a dam on a river that originates in a certain country and flows to other countries can have a positive effect on the source country and negative effects on the vegetation of countries located downriver. The Ilisu Dam, constructed on the Tigris River, harms the vegetation in Syria, Iraq and Iran.

The results of this study can be used by policymakers in the ME to closely examine the vegetation dynamics and their variations in each region and country. Studying the NDVI dynamics and their relationship with vegetation growth, and monitoring in this region is very important for ensuring agricultural, hydroecological, and environmental sustainability, and food security; it is also necessary for formulating effective intergovernmental policies.

The main limitation of the presented results is the resolution of the Terra-MODIS Vegetation Indices MOD13A1 grid (500 x 500 m), which may be too coarse and be a source of error. Further

 doi:10.20944/preprints202010.0208.v2

research should be carried out on ME vegetation dynamics, incorporating datasets with higher spatial resolution, historical vegetation dynamics, and their correlations with the atmospheric variability and land–atmosphere interactions in this environmentally sensitive territory.

Author Contributions: I.R. proposed the study. I.R., H.O., H.Z., and Md.M. carried out the data processing and analysis and wrote the manuscript. J.K. and P.B. enhanced the research design, helped with the analysis and interpretation of the results, and helped with writing the manuscript.

Funding: This research was supported by Vedurfelagid, Rannis, and Rannsoknastofa i vedurfraedi. J.K. and P.B. have been partly financed by the Polish National Centre for Research and Development within the framework of the MSINiN project (contract number: BIOSTRATEG3/343547/8/NCBR/2017).

Conflicts of Interest: The authors declare no conflicts of interest. The funding bodies played no roles in the design of the study; in the collection, analyses, or interpretation of data; in the writing of the manuscript; nor in the decision to publish the results.

References

1. Anderson, R.G.; Canadell, J.G.; Randerson, J.T.; Jackson, R.B.; Hungate, B.A.; Baldocchi, D.D.; Ban-Weiss, G.A.; Bonan, G.B.; Caldeira, K.; Cao, L. Biophysical considerations in forestry for climate protection. *Front. Ecol. Environ* **2011**, *9*, 174-182.
2. Cramer, W.; Bondeau, A.; Woodward, F.I.; Prentice, I.C.; Betts, R.A.; Brovkin, V.; Cox, P.M.; Fisher, V.; Foley, J.A.; Friend, A.D. Global response of terrestrial ecosystem structure and function to CO_2 and climate change: results from six dynamic global vegetation models. *Glob. Chang. Biol.* **2001**, *7*, 357-373.
3. Gaston, K.J. Global patterns in biodiversity. *Nature* **2000**, *405*, 220-227.
4. Guo, W.; Ni, X.; Jing, D.; Li, S. Spatial-temporal patterns of vegetation dynamics and their relationships to climate variations in Qinghai Lake Basin using MODIS time-series data. *J. Geogr. Sci.* **2014**, *24*, 1009-1021.
5. Jackson, R.B.; Randerson, J.T.; Canadell, J.G.; Anderson, R.G.; Avissar, R.; Baldocchi, D.D.; Bonan, G.B.; Caldeira, K.; Diffenbaugh, N.S.; Field, C.B. Protecting climate with forests. *Environ. Res. Lett.* **2008**, *3*, 044006.
6. Theurillat, J.-P.; Guisan, A. Potential impact of climate change on vegetation in the European Alps: a review. *Clim. Change* **2001**, *50*, 77-109.
7. Verbesselt, J.; Hyndman, R.; Newnham, G.; Culvenor, D. Detecting trend and seasonal changes in satellite image time series. *Remote Sens. Environ.* **2010**, *114*, 106-115.
8. Wolters, V.; Silver, W.L.; Bignell, D.E.; Coleman, D.C.; Lavelle, P.; Van Der Putten, W.H.; De Ruiter, P.; Rusek, J.; Wall, D.H.; Wardle, D.A. Effects of Global Changes on Above-and Belowground Biodiversity in Terrestrial Ecosystems: Implications for Ecosystem Functioning: We identify the basic types of interaction between vascular plants and soil biota; describe the sensitivity of each type to changes in species composition; and, within this framework, evaluate the potential consequences of global change drivers on ecosystem processes. *Bioscience* **2000**, *50*, 1089-1098.
9. Chuai, X.; Huang, X.; Wang, W.; Bao, G. NDVI, temperature and precipitation changes and their relationships with different vegetation types during 1998–2007 in Inner Mongolia, China. *Int. J. Climatol.* **2013**, *33*, 1696-1706.
10. Wang, J.; Rich, P.M.; Price, K.P. Temporal responses of NDVI to precipitation and temperature in the central Great Plains, USA. *Int. J. Remote Sens.* **2003**, *24*, 2345-2364.
11. Badreldin, N.; Goossens, R. Monitoring land use/land cover change using multi-temporal Landsat satellite images in an arid environment: a case study of El-Arish, Egypt. *Arab. J. Geosci.* **2014**, *7*, 1671-1681.
12. Bagherzadeh, A.; Hoseini, A.V.; Totmaj, L.H. The effects of climate change on normalized difference vegetation index (NDVI) in the Northeast of Iran. *Model. Earth Syst. Environ.* **2020**, *6*, 671-683.
13. Cui, L.; Shi, J. Temporal and spatial response of vegetation NDVI to temperature and precipitation in eastern China. *J. Geogr. Sci.* **2010**, *20*, 163-176.
14. Schultz, P.; Halpert, M.S. Global correlation of temperature, NDVI and precipitation. *Adv. Space Res.* **1993**, *13*, 277-280.
15. Schultz, P.; Halpert, M.S. Global analysis of the relationships among a vegetation index, precipitation and land surface temperature. *Int. J. Remote Sens.* **1995**, *16*, 2755-2777.
16. Zhang, G.; Xu, X.; Zhou, C.; Zhang, H.; Ouyang, H. Responses of grassland vegetation to climatic variations on different temporal scales in Hulun Buir Grassland in the past 30 years. *J. Geogr. Sci.* **2011**, *21*, 634-650.

17. Li, X.; Jia, X.; Dong, G. Influence of desertification on vegetation pattern variations in the cold semi-arid grasslands of Qinghai-Tibet Plateau, North-west China. *J. Arid Environ.* **2006**, *64*, 505-522.
18. Lucas, R.; Rowlands, A.; Brown, A.; Keyworth, S.; Bunting, P. Rule-based classification of multi-temporal satellite imagery for habitat and agricultural land cover mapping. *ISPRS J. Photogramm. Remote Sens.* **2007**, *62*, 165-185.
19. Tong, X.; Wang, K.; Yue, Y.; Brandt, M.; Liu, B.; Zhang, C.; Liao, C.; Fensholt, R. Quantifying the effectiveness of ecological restoration projects on long-term vegetation dynamics in the karst regions of Southwest China. *Int. J. Appl. Earth Obs. Geoinf.* **2017**, *54*, 105-113.
20. Xiao, X.; Wang, Y.; Jiang, S.; Ojima, D.S.; Bonham, C.D. Interannual variation in the climate and above-ground biomass of Leymus chinense steppe and Stipa grandis steppe in the Xilin river basin, Inner Mongolia, China. *J. Arid Environ.* **1995**, *31*, 283-299.
21. Bradley, B.A.; Mustard, J.F. Comparison of phenology trends by land cover class: a case study in the Great Basin, USA. *Glob. Chang. Biol.* **2008**, *14*, 334-346.
22. Frolking, S.; Palace, M.W.; Clark, D.; Chambers, J.Q.; Shugart, H.; Hurtt, G.C. Forest disturbance and recovery: A general review in the context of spaceborne remote sensing of impacts on aboveground biomass and canopy structure. *J. Geophys. Res. Biogeosci.* **2009**, *114*, G00E02.
23. Fu, B.; Burgher, I. Riparian vegetation NDVI dynamics and its relationship with climate, surface water and groundwater. *J. Arid Environ.* **2015**, *113*, 59-68.
24. Ghafarian Malamiri, H.R.; Rousta, I.; Olafsson, H.; Zare, H.; Zhang, H. Gap-Filling of MODIS Time Series Land Surface Temperature (LST) Products Using Singular Spectrum Analysis (SSA). *Atmosphere* **2018**, *9*, 334.
25. Guillevic, P.; Koster, R.; Suarez, M.; Bounoua, L.; Collatz, G.; Los, S.; Mahanama, S. Influence of the interannual variability of vegetation on the surface energy balance—A global sensitivity study. *J. Hydrometeorol.* **2002**, *3*, 617-629.
26. Gupta, A.; Moniruzzaman, M.; Hande, A.; Rousta, I.; Olafsson, H.; Mondal, K.K. Estimation of particulate matter ($PM_{2.5}$, PM_{10}) concentration and its variation over urban sites in Bangladesh. *SN Appl. Sci.* **2020**, *2(1993)*, 1-15.
27. Höpfner, C.; Scherer, D. Analysis of vegetation and land cover dynamics in north-western Morocco during the last decade using MODIS NDVI time series data. *Biogeosciences* **2011**, *8*, 3359-3373.
28. Ludwig, J.A.; Bastin, G.N.; Chewings, V.H.; Eager, R.W.; Liedloff, A.C. Leakiness: a new index for monitoring the health of arid and semiarid landscapes using remotely sensed vegetation cover and elevation data. *Ecol. Indic.* **2007**, *7*, 442-454.
29. Lunetta, R.S.; Knight, J.F.; Ediriwickrema, J.; Lyon, J.G.; Worthy, L.D. Land-cover change detection using multi-temporal MODIS NDVI data. *Remote Sens. Environ.* **2006**, *105*, 142-154.
30. Moniruzzaman, M.; Roy, A.; Bhatt, C.M.; Gupta, A.; An, N.T.T.; Hassan, M.R. Impact Analysis of Urbanization on Land Use Land Cover Change for Khulna City, Bangladesh Using Temporal Landsat Imagery. *Int. Arch. Photogramm. Remote Sens. Spatial Inf. Sci.* **2018**, *XLII-5*, 757-760.
31. Mushore, T.D.; Dube, T.; Manjowe, M.; Gumindoga, W.; Chemura, A.; Rousta, I.; Odindi, J.; Mutanga, O. Remotely sensed retrieval of Local Climate Zones and their linkages to land surface temperature in Harare metropolitan city, Zimbabwe. *Urban Clim.* **2019**, *27*, 259-271.
32. Tucker, C.J.; Slayback, D.A.; Pinzon, J.E.; Los, S.O.; Myneni, R.B.; Taylor, M.G. Higher northern latitude normalized difference vegetation index and growing season trends from 1982 to 1999. *Int. J. Biometeorol.* **2001**, *45*, 184-190.
33. White, A.B.; Kumar, P.; Tcheng, D. A data mining approach for understanding topographic control on climate-induced inter-annual vegetation variability over the United States. *Remote Sens. Environ.* **2005**, *98*, 1-20.
34. Zhao, B.; Yan, Y.; Guo, H.; He, M.; Gu, Y.; Li, B. Monitoring rapid vegetation succession in estuarine wetland using time series MODIS-based indicators: an application in the Yangtze River Delta area. *Ecol. Indic.* **2009**, *9*, 346-356.
35. Justice, C.O.; Vermote, E.; Townshend, J.R.; Defries, R.; Roy, D.P.; Hall, D.K.; Salomonson, V.V.; Privette, J.L.; Riggs, G.; Strahler, A. The Moderate Resolution Imaging Spectroradiometer (MODIS): Land remote sensing for global change research. *IEEE Trans. Geosci. Remote Sens.* **1998**, *36*, 1228-1249.
36. Dineshkumar, C.; Nitheshnirmal, S.; Bhardwaj, A.; Priyadarshini, K.N. Phenological Monitoring of Paddy Crop Using Time Series MODIS Data. *Proceedings* ***2019***, *24*, 19, 1-6.

37. Rousta, I.; Olafsson, H.; Moniruzzaman, M.; Zhang, H.; Liou, Y.-A.; Mushore, T.D.; Gupta, A. Impacts of Drought on Vegetation Assessed by Vegetation Indices and Meteorological Factors in Afghanistan. *Remote Sens.* **2020**, *12*, 2433.
38. Fensholt, R.; Sandholt, I.; Rasmussen, M.S. Evaluation of MODIS LAI, fAPAR and the relation between fAPAR and NDVI in a semi-arid environment using in situ measurements. *Remote Sens. Environ.* **2004**, *91*, 490-507.
39. Ichii, K.; Kawabata, A.; Yamaguchi, Y. Global correlation analysis for NDVI and climatic variables and NDVI trends: 1982-1990. *Int. J. Remote Sens.* **2002**, *23*, 3873-3878.
40. Pettorelli, N.; Vik, J.O.; Mysterud, A.; Gaillard, J.-M.; Tucker, C.J.; Stenseth, N.C. Using the satellite-derived NDVI to assess ecological responses to environmental change. *Trends Ecol. Evol.* **2005**, *20*, 503-510.
41. Reed, B.C.; Brown, J.F.; VanderZee, D.; Loveland, T.R.; Merchant, J.W.; Ohlen, D.O. Measuring phenological variability from satellite imagery. *J. Veg. Sci.* **1994**, *5*, 703-714.
42. Faisal, B.; Rahman, H.; Sharifee, N.H.; Sultana, N.; Islam, M.I.; Ahammad, T. Remotely Sensed Boro Rice Production Forecasting Using MODIS-NDVI: A Bangladesh Perspective. *AgriEngineering* **2019**, *1*, 356-375.
43. Rousta, I.; Olafsson, H.; Moniruzzaman, M.; Ardö, J.; Zhang, H.; Mushore, T.D.; Shahin, S.; Azim, S. The 2000–2017 drought risk assessment of the western and southwestern basins in Iran. *Model. Earth Syst. Environ.* **2020**, *6*, 1201-1221.
44. Schnur, M.T.; Xie, H.; Wang, X. Estimating root zone soil moisture at distant sites using MODIS NDVI and EVI in a semi-arid region of southwestern USA. *Ecol. Inform.* **2010**, *5*, 400-409.
45. Busetto, L.; Meroni, M.; Colombo, R. Combining medium and coarse spatial resolution satellite data to improve the estimation of sub-pixel NDVI time series. *Remote Sens. Environ.* **2008**, *112*, 118-131.
46. Sims, N.C.; Colloff, M.J. Remote sensing of vegetation responses to flooding of a semi-arid floodplain: Implications for monitoring ecological effects of environmental flows. *Ecol. Indic.* **2012**, *18*, 387-391.
47. Cho, M.A.; Skidmore, A.; Corsi, F.; Van Wieren, S.E.; Sobhan, I. Estimation of green grass/herb biomass from airborne hyperspectral imagery using spectral indices and partial least squares regression. *Int. J. Appl. Earth Obs. Geoinf.* **2007**, *9*, 414-424.
48. Rouse, J.; Haas, R.; Schell, J.; Deering, D. Monitoring vegetation systems in the Great Plains with ERTS. *NASA special publication* **1974**, *351*, 309.
49. Goward, S.N.; Dye, D.G. Evaluating North American net primary productivity with satellite observations. *Adv. Space Res.* **1987**, *7*, 165-174.
50. Nielsen, T.T.; Adriansen, H.J.L.D. Government policies and land degradation in the Middle East. *Land Degrad. Dev.* **2005**, *16*, 151-161.
51. Barbosa, H.; Huete, A.; Baethgen, W. A 20-year study of NDVI variability over the Northeast Region of Brazil. *J. Arid Environ.* **2006**, *67*, 288-307.
52. Gaughan, A.E.; Stevens, F.R.; Gibbes, C.; Southworth, J.; Binford, M.W. Linking vegetation response to seasonal precipitation in the Okavango–Kwando–Zambezi catchment of southern Africa. *Int. J. Remote Sens.* **2012**, *33*, 6783-6804.
53. Ji, L.; Peters, A.J. Assessing vegetation response to drought in the northern Great Plains using vegetation and drought indices. *Remote Sens. Environ.* **2003**, *87*, 85-98.
54. Zaitchik, B.F.; Evans, J.P.; Geerken, R.A.; Smith, R.B.J.J.o.C. Climate and vegetation in the Middle East: Interannual variability and drought feedbacks. *J. Climate* **2007**, *20*, 3924-3941.
55. Archer, E.R. Beyond the "climate versus grazing" impasse: using remote sensing to investigate the effects of grazing system choice on vegetation cover in the eastern Karoo. *J. Arid Environ.* **2004**, *57*, 381-408.
56. Herrmann, S.M.; Anyamba, A.; Tucker, C.J. Recent trends in vegetation dynamics in the African Sahel and their relationship to climate. *Glob. Environ. Change* **2005**, *15*, 394-404.
57. Pinzon, J.E.; Tucker, C.J. A non-stationary 1981–2012 AVHRR NDVI3g time series. *Remote Sens.* **2014**, *6*, 6929-6960.
58. Running, S.W.; Nemani, R.R. Relating seasonal patterns of the AVHRR vegetation index to simulated photosynthesis and transpiration of forests in different climates. *Remote Sens. Environ.* **1988**, *24*, 347-367.
59. Cai, H.; Yang, X.; Wang, K.; Xiao, L. Is forest restoration in the southwest China Karst promoted mainly by climate change or human-induced factors? *Remote Sens.* **2014**, *6*, 9895-9910.
60. Wang, J.; Meng, J.; Cai, Y. Assessing vegetation dynamics impacted by climate change in the southwestern karst region of China with AVHRR NDVI and AVHRR NPP time-series. *Environ. Geol.* **2008**, *54*, 1185-1195.

61. Evans, J.; Geerken, R. Discrimination between climate and human-induced dryland degradation. *J. Arid Environ.* **2004**, *57*, 535-554.
62. Quaye-Ballard, J.A.; Okrah, T.M.; Andam-Akorful, S.A.; Awotwi, A.; Osei-Wusu, W.; Antwi, T.; Tang, X. Assessment of vegetation dynamics in Upper East Region of Ghana based on wavelet multi-resolution analysis. *Model. Earth Syst. Environ.* **2020**, *6*, 1783-1793.
63. Zhang, W.; Wang, L.; Xiang, F.; Qin, W.; Jiang, W. Vegetation dynamics and the relations with climate change at multiple time scales in the Yangtze River and Yellow River Basin, China. *Ecol. Indic.* **2020**, *110*, 105892.
64. Jiang, H.; Xu, X.; Guan, M.; Wang, L.; Huang, Y.; Jiang, Y. Determining the contributions of climate change and human activities to vegetation dynamics in agro-pastural transitional zone of northern China from 2000 to 2015. *Sci. Total Environ.* **2020**, *718*, 134871.
65. Hameed, M.; Ahmadalipour, A.; Moradkhani, H. Drought and food security in the middle east: An analytical framework. *Agric. For. Meteorol.* **2020**, *281*, 107816.
66. Lelieveld, J.; Hadjinicolaou, P.; Kostopoulou, E.; Chenoweth, J.; El Maayar, M.; Giannakopoulos, C.; Hannides, C.; Lange, M.A.; Tanarhte, M.; Tyrlis, E.; Xoplaki, E. Climate change and impacts in the Eastern Mediterranean and the Middle East. *Clim. Change* **2012**, *114*, 667-687.
67. Ahmadalipour, A.; Moradkhani, H.; Escalating heat-stress mortality risk due to global warming in the Middle East and North Africa (MENA). *Environ. Int.* **2018**, *117*, 215-225.
68. Amiraslani F; Dragovich D. Combating desertification in Iran over the last 50 years: an overview of changing approaches. *J. Environ. Manag.* **2011**, *92*, 1-13.
69. Hameed, M.; Moradkhani, H.; Ahmadalipour, A.; Moftakhari, H.; Abbaszadeh, P.; Alipour, A. A review of the 21st century challenges in the food-energy-water security in the Middle East. *Water* **2019**, *11*, 682.
70. Badreldin, N.; Goossens, R. A satellite-based disturbance index algorithm for monitoring mitigation strategies effects on desertification change in an arid environment. *Mitig. Adapt. Strateg. Glob. Change* **2015**, *20*, 263-276.
71. Fisher, L. *Presidential war power*, 3rd ed.; Publisher: University Press of Kansas, 2013
72. Budhwar, P.; Mellahi, K. Introduction: human resource management in the Middle East. *Int. J. Hum. Resour. Manag.* **2007**, *18*, 2-10.
73. Budhwar, P.; Mellahi, K. HRM in the Middle East. In *Handbook of Research on Comparative Human Resource Management*, 2nd ed.; Publisher: Edward Elgar Publishing, 2018.
74. Didan, K.; Munoz, A.B.; Solano, R.; Huete, A. MODIS vegetation index user's guide (MOD13 series) version 3.00 (Collection 6). *University of Arizona: Vegetation Index and Phenology Lab* **2015**.
75. Loveland, T.R.; Zhu, Z.; Ohlen, D.O.; Brown, J.F.; Reed, B.C.; Yang, L. An analysis of the IGBP global land-cover characterization process. *Photogramm. Eng. Remote Sensing* **1999**, *65*, 1021-1032.
76. Huffman, G.; Bolvin, D.; Braithwaite, D.; Hsu, K.; Joyce, R.; Xie, P. 2014: GPM Integrated Multi-Satellite Retrievals for GPM (IMERG) Algorithm Theoretical Basis Document (ATBD) Version 4.4, NASA/GSFC, 2014, pp. 1-30. http://pmm.nasa.gov/sites/default/files/document_files/IMERG_ATBD_V4.4.pdf.
77. Huffman, G.; Stocker, E.; Bolvin, D.; Nelkin, E.; Jackson, T. GPM IMERG Final Precipitation L3 Half Hourly 0.1 degree x 0.1 degree V06, Greenbelt, MD, Goddard Earth Sciences Data and Information Services Center (GES DISC), 2019.
78. Rodell, M.; Houser P.R.; Jambor U.; Gottschalck J.; Mitchell K.; Meng C.-J.; Arsenault K.; Cosgrove B.; Radakovich J.; Bosilovich M.; Entin J.K.; Walker J.P.; Lohmann D.; Toll D. The Global Land Data Assimilation System. *Bull. Amer. Meteor. Soc.* **2004**, *85*, 381-394.
79. Zandbergen, P. Applications of shuttle radar topography mission elevation data. *Geogr. Compass* **2008**, *2*, 1404-1431.
80. Wickland, D.E. Mission to Planet Earth: The Ecological Perspective. *Ecology* **1991**, *72*, 1923-1933
81. Dutta, D.; Kundu, A.; Patel, N.; Saha, S.; Siddiqui, A. Assessment of agricultural drought in Rajasthan (India) using remote sensing derived Vegetation Condition Index (VCI) and Standardized Precipitation Index (SPI). *Egypt. J. Remote. Sens. Space Sci.* **2015**, *18*, 53-63.
82. Gitelson, A.A.; Viña, A.; Arkebauer, T.J.; Rundquist, D.C.; Keydan, G.; Leavitt, B. Remote estimation of leaf area index and green leaf biomass in maize canopies. *Geophys. Res. Lett.* **2003**, *30*, 1248.
83. Tarpley, J.; Schneider, S.; Money, R. Global vegetation indices from the NOAA-7 meteorological satellite. *J. Clim. Appl. Meteorol.* **1984**, *23*, 491-494.

84. Thenkabail, P.S.; Gamage, M. *The use of remote sensing data for drought assessment and monitoring in Southwest Asia*; Publisher: International Water Management Institute, 2004.
85. Geerken, R.; Zaitchik, B.; Evans, J. Classifying rangeland vegetation type and coverage from NDVI time series using Fourier Filtered Cycle Similarity. *Int. J. Remote Sens.* **2005**, *26*, 5535-5554.
86. Martínez, B.; Gilabert, M. Vegetation dynamics from NDVI time series analysis using the wavelet transform. *Remote Sens. Environ.* **2009**, *113*, 1823-1842.
87. Moulin, S.; Kergoat, L.; Viovy, N.; Dedieu, G. Global-scale assessment of vegetation phenology using NOAA/AVHRR satellite measurements. *J. Climate* **1997**, *10*, 1154-1170.
88. Running, S.W.; Loveland, T.R.; Pierce, L.L.; Nemani, R.R.; Hunt Jr, E. A remote sensing based vegetation classification logic for global land cover analysis. *Remote Sens. Environ.* **1995**, *51*, 39-48.
89. Townshend, J.R.; Justice, C. Analysis of the dynamics of African vegetation using the normalized difference vegetation index. *Int. J. Remote Sens.* **1986**, *7*, 1435-1445.
90. Bhandari, A.; Kumar, A.; Singh, G. Feature extraction using Normalized Difference Vegetation Index (NDVI): A case study of Jabalpur city. *Proc. Technol.* **2012**, *6*, 612-621.
91. Cai, D.; Fraedrich, K.; Sielmann, F.; Guan, Y.; Guo, S.; Zhang, L.; Zhu, X. Climate and vegetation: An ERA-interim and GIMMS NDVI analysis. *J. Clim.* **2014**, *27*, 5111-5118.
92. Chuvieco, E.; Cocero, D.; Riano, D.; Martin, P.; Martınez-Vega, J.; de la Riva, J.; Pérez, F. Combining NDVI and surface temperature for the estimation of live fuel moisture content in forest fire danger rating. *Remote Sens. Environ.* **2004**, *92*, 322-331.
93. Gandhi, G.M.; Parthiban, S.; Thummalu, N.; Christy, A. Ndvi: Vegetation change detection using remote sensing and gis–A case study of Vellore District. *Procedia Comput. Sci.* **2015**, *57*, 1199-1210.
94. Goward, S.N.; Markham, B.; Dye, D.G.; Dulaney, W.; Yang, J. Normalized difference vegetation index measurements from the Advanced Very High Resolution Radiometer. *Remote Sens. Environ.* **1991**, *35*, 257-277.
95. Didan, K. 2015. MOD13Q1 MODIS/Terra vegetation indices 16-day L3 global 250m SIN grid V006. NASA EOSDIS Land Processes DAAC.
96. Weier, J.; Herring, D. Measuring vegetation (NDVI & EVI). *NASA Earth Observatory* **2000**, 20.
97. Wang, R.; Cherkauer, K.; Bowling, L. Corn Response to Climate Stress Detected with Satellite-Based NDVI Time Series. *Remote Sens.* **2016**, *8*, 269.
98. Deng, G.; Zhang, H.; Guo, X.; Ying, H. Assessment of Drought in Democratic People's Republic of Korea in 2017 Using TRMM Data. In: Proceedings of 2018 Fifth International Workshop on Earth Observation and Remote Sensing Applications (EORSA), Xi'an, 2018, pp. 1-5.
99. Duan, Z.; Bastiaanssen, W. First results from Version 7 TRMM 3B43 precipitation product in combination with a new downscaling–calibration procedure. *Remote Sens. Environ.* **2013**, *131*, 1-13.
100. Mossad, A.; Alazba, A. Determination and prediction of standardized precipitation index (SPI) using TRMM data in arid ecosystems. *Arab. J. Geosci.* **2018**, *11(132)*, 1-16.
101. Nastos, P.; Kapsomenakis, J.; Philandras, K. Evaluation of the TRMM 3B43 gridded precipitation estimates over Greece. *Atmos. Res.* **2016**, *169*, 497-514.
102. Skofronick-Jackson, G.; Kirschbaum, D.; Petersen, W.; Huffman, G.; Kidd, C.; Stocker, E.; Kakar, R. The Global Precipitation Measurement (GPM) mission's scientific achievements and societal contributions: reviewing four years of advanced rain and snow observations. *Q. J. R. Meteorol. Soc.* **2018**, *144*, 27-48.
103. Almazroui, M. Calibration of TRMM rainfall climatology over Saudi Arabia during 1998–2009. *Atmos. Res.* **2011**, *99*, 400-414.
104. Kummerow, C.; Barnes, W.; Kozu, T.; Shiue, J.; Simpson, J. The tropical rainfall measuring mission (TRMM) sensor package. *J. Atmos. Oceanic Tech.* **1998**, *15*, 809-817.
105. Patel, N.; Chopra, P.; Dadhwal, V. Analyzing spatial patterns of meteorological drought using standardized precipitation index. *Met. Apps* **2007**, *14*, 329-336.
106. Stevens-Rumann, C.S.; Kemp, K.B.; Higuera, P.E.; Harvey, B.J.; Rother, M.T.; Donato, D.C.; Morgan, P.; Veblen, T.T. Evidence for declining forest resilience to wildfires under climate change. *Ecol. Lett.* **2018**, *21*, 243-252.
107. Raja, R.; Nayak, A.; Panda, B.; Lal, B.; Tripathi, R.; Shahid, M.; Kumar, A.; Mohanty, S.; Samal, P.; Gautam, P. Monitoring of meteorological drought and its impact on rice (Oryza sativa L.) productivity in Odisha using standardized precipitation index. *Arch. Agron. Soil Sci.* **2014**, *60*, 1701-1715.

108. Dahiru, T. P-value, a true test of statistical significance? A cautionary note. *Ann. Ib. Postgrad. Med.* **2008**, *6*, 21-26.
109. Eberly, L.E. Correlation and simple linear regression. *Methods Mol. Biol.* **2007**, *404*, 143-164.
110. Zou, K.H.; Tuncali, K.; Silverman, S.G. Correlation and simple linear regression. *Radiology* **2003**, *227*, 617-628.
111. Allan, J.A. Fortunately there are substitutes for water otherwise our hydropolitical futures would be impossible. In: Proceedings of the conference on Priorities for Water Resources Allocation and Management; Overseas Development Administration (ODA), London, UK, 1993, pp. 13-26.
112. Sofroniou, A.; Bishop, S. Water Scarcity in Cyprus: A Review and Call for Integrated Policy. *Water* **2014**, *6*, 2898-2928.
113. Li, J.; Chou, J. Dynamical analysis on splitting of subtropical high-pressure zone. *Chin. Sci. Bull.* **1998**, *43*, 1285-1289.
114. Najafi, M.S.; Sarraf, B.; Zarrin, A.; Rasouli, A. Climatology of atmospheric circulation patterns of Arabian dust in western Iran. *Environ. Monit. Assess.* **2017**, *189*, 473.
115. Rousta, I.; Doostkamian, M.; Haghighi, E.; Mirzakhani, B. Statistical-synoptic analysis of the atmosphere thickness pattern of iran's pervasive frosts. *Climate* **2016**, *4*, 41.
116. Rousta, I.; Karampour, M.; Doostkamian, M.; Olafsson, H.; Zhang, H.; Mushore, T.D.; Karimvandi, A.S.; Vargas, E.R.M. Synoptic-dynamic analysis of extreme precipitation in Karoun River Basin, Iran. *Arab. J. Geosci.* **2020**, *13*, 1-16.
117. Bolin, B. On the influence of the earth's orography on the general character of the westerlies. *Tellus* **1950**, *2*, 184-195.
118. Toggweiler, J. Shifting westerlies. *Science* **2009**, *323*, 1434-1435.
119. Rousta, I.; Nasserzadeh, M.H.; Jalali, M.; Haghighi, E.; Ólafsson, H.; Ashrafi, S.; Doostkamian, M.; Ghasemi, A. Decadal spatial-temporal variations in the spatial pattern of anomalies of extreme precipitation thresholds (Case Study: Northwest Iran). *Atmosphere* **2017**, *8*, 135.
120. Rousta, I.; Javadizadeh, F.; Dargahian, F.; Olafsson, H.; Shiri-Karimvandi, A.; Vahedinejad, S.H.; Doostkamian, M.; Monroy Vargas, E.R.; Asadolahi, A. Investigation of vorticity during prevalent winter precipitation in Iran. *Adv. Meteorol.* **2018**, *6941501*, 1-13.
121. Rousta, I.; Doostkamian, M.; Ólafsson, H.; Zhang, H.; Vahedinejad, S.H.; Sarif, M.O.; Monroy Vargas, E.R. Analyzing the fluctuations of atmospheric precipitable water in Iran during various periods based on the retrieving technique of NCEP/NCAR. *Open Atmospheric Sci. J.* **2018**, 12, 48-57.
122. Rousta, I.; Doostkamian, M.; Olafsson, H.; Ghafarian-Malamiri, H.; Zhang, H.; Taherian, A.; Sarif, M.; Gupta, R.; Monroy-Vargas, E. On the relationship between the 500 hPa height fluctuations and the atmosphere thickness over Iran and the Middle East. *Tethys* **2019**, *16*, 3-14.
123. Elbana, T.A.; Bakr, N.; Elbana, M. Reuse of treated wastewater in Egypt: challenges and opportunities. In: Unconventional Water Resources and Agriculture in Egypt. The Handbook of Environmental Chemistry, Negm, A., Eds. Springer: Cham., 2017, 75, pp. 429-453.
124. Abdel-Shafy, H.I.; Mansour, M.S. Overview on water reuse in Egypt: present and future. *Sustainable Sanitation Practice* **2013**, *14*, 17-25.
125. Loutfy, N.M. Reuse of Wastewater in Mediterranean Region, Egyptian Experience. In: Waste Water Treatment and Reuse in the Mediterranean Region, Barceló, D., Petrovic, M., Eds. Springer Berlin Heidelberg: Berlin, Heidelberg, 2011, pp. 183-213.
126. Ewaid, S.H.; Abed, S.A.; Al-Ansari, N. Water Footprint of Wheat in Iraq. *Water* **2019**, *11*, 535.
127. Bilgen, A. The Southeastern Anatolia Project (GAP) revisited: The evolution of GAP over forty years. *New Perspect. Turk.* **2018**, *58*, 125-154.
128. Özcan, O.; Bookhagen, B.; Musaoğlu, N. Impact of the Atatürk dam lake on agro-meteorological aspects of the southeastern Anatolia region, Turkey. *J. Indian Soc. Remote. Sens.* **2018**, *46*, 471-481.\
129. Al-Madhhachi, A.-S.T.; Rahi, K.A.; Leabi, W.K. Hydrological Impact of Ilisu Dam on Mosul Dam; the River Tigris. *Geosciences* **2020**, *10*, 120.
130. Kankal, M.; Nacar, S.; Uzlu, E. Status of hydropower and water resources in the Southeastern Anatolia Project (GAP) of Turkey. *Energy Rep.* **2016**, *2*, 123-128.
131. Frenken, K. Legislative and institutional framework of water management. In: Irrigation in the middle east region in figures. AQUASTAT survey. *FAO Water Reports* **2008**, *34*, 55–56.

132. Abdel-Satar, A.M.; Al-Khabbas, M.H.; Alahmad, W.R.; Yousef, W.M.; Alsomadi, R.H.; Iqbal, T. Quality assessment of groundwater and agricultural soil in Hail region, Saudi Arabia. *Egypt. J. Aquat. Res.* **2017**, *43*, 55-64.
133. Fiaz, S.; Noor, M.A.; Aldosri, F.O. Achieving food security in the Kingdom of Saudi Arabia through innovation: Potential role of agricultural extension. *J. Saudi Soc. Agric. Sci.* **2018**, *17*, 365-375.